Coordinated airborne, spaceborne, and ground-based measurements of massive, thick aerosol layers during the dry season in Southern Africa

B. Schmid,[1] J. Redemann,[1] P. B. Russell,[2] P. V. Hobbs,[3] D. L. Hlavka,[4] M. J. McGill,[5]

B. N. Holben,[5] E. J. Welton,[6] J. Campbell,[4] O. Torres,[7] R. A. Kahn,[8] D. J. Diner,[8]

M. C. Helmlinger,[8] D. A. Chu,[4] C. Robles Gonzalez,[9] and G. de Leeuw[9]

Submitted to JGR SAFARI 2000 Special Issue, March 13 2002.

Last changed: 5/31/2002 3:37 PM

Corresponding author: Beat Schmid

Bay Area Environmental Research Institute

NASA Ames Research Center

MS 245-5

Moffett Field, CA 94035-1000

Phone: +1 650 604 5933

Fax: +1 650 604 3625

e-mail: bschmid@mail.arc.nasa.gov

Affiliations:

[1] Bay Area Environmental Research Institute, 645 Anthony Court, Sonoma, CA 95476. (e-mail: bschmid@mail.arc.nasa.gov, jredemann@mail.arc.nasa.gov)

[2] NASA Ames Research Center, MS 245-5, Moffett Field, CA 94035-1000. (e-mail: prussell@mail.arc.nasa.gov)

[3] Department of Atmospheric Sciences, University of Washington, Box 351640, Seattle, WA 98195-1640. (e-mail: phobbs@atmos.washington.edu)

[4] Science Systems and Applications, Inc., NASA Goddard Space Flight Center, Greenbelt, MD 20771. (e-mail: sgdlh@virl.gsfc.nasa.gov, campbell@virl.gsfc.nasa.gov, chu@climate.gsfc.nasa.gov)

[5] NASA Goddard Space Flight Center, Greenbelt, MD 20771. (e-mail: mcgill@virl.gsfc.nasa.gov, brent@aeronet.gsfc.nasa.gov

[6] Goddard Earth Sciences & Technology Center, NASA Goddard Space Flight Center, Code 912, Greenbelt, MD 20771. (e-mail: welton@virl.gsfc.nasa.gov)

[7] Joint Center for Earth Systems, University of Maryland, Baltimore County, NASA Goddard Space Flight Center, Code 916, Greenbelt, MD 20771. (e-mail: torres@tparty.gsfc.nasa.gov)

[8] Jet Propulsion Laboratory, California Institute of Technology, 4800 Oak Grove Drive, Pasadena, CA 91109-8099. (e-mail Ralph.A.Kahn@jpl.nasa.gov, David.J.Diner@jpl.nasa.gov, Mark.C.Helmlinger@jpl.nasa.gov)

[9]TNO Physics and Electronics Laboratory, P.O. Box 96864, 2509 JG, The Hague, The Netherlands. (e-mail: Robles-Gonzalez@fel.tno.nl, deleeuw@fel.tno.nl)

Abstract

During the dry-season airborne campaign of the Southern African Regional Science Initiative (SAFARI 2000), coordinated observations were made of massive, thick aerosol layers. These layers were often dominated by aerosols from biomass burning. We report on airborne Sunphotometer measurements of aerosol optical depth (λ=0.354-1.557 μm), columnar water vapor, and vertical profiles of aerosol extinction and water vapor density that were obtained aboard the University of Washington's Convair-580 research aircraft. We compare these with ground-based AERONET Sun/sky radiometer results, with ground based lidar data (MPL-Net), and with measurements from a downward-pointing lidar aboard the high-flying NASA ER-2 aircraft. Finally, we show comparisons between aerosol optical depths from the Sunphotometer and those retrieved over land and over water using four spaceborne sensors (TOMS, MODIS, MISR and ATSR-2).

1. Introduction

From August 13 to September 25, 2000, the Southern African Regional Science Initiative's (SAFARI 2000) dry-season airborne campaign coordinated ground-based measurement teams, multiple research aircraft, and satellite overpasses across nine African nations [*Swap et al*., this issue]. Among many other accomplishments, coordinated observations were made of the evolution of massive, thick haze layers produced by biomass burning, industrial emissions, and biogenic and marine sources.

During SAFARI 2000, the NASA Ames Airborne Tracking 14-channel Sunphotometer (AATS-14) was operated aboard the University of Washington's (UW) Convair-580 research aircraft [*Hobbs*, this issue, a]. The AATS-14 measures the transmission of the direct solar beam

at 14 discrete wavelengths from 0.354 to 1.557 μm from which spectral aerosol optical depths $\tau_a(\lambda)$, columnar water vapor (CWV) and columnar ozone can be derived. Flying at different altitudes over a fixed location allows derivation of layer $\tau_a(\lambda)$ or CWV. Data obtained in vertical profiles allows derivation of spectral aerosol extinction $E_a(\lambda)$ and water vapor density ρ_w.

Here we discuss a subset of AATS-14 results from 24 data flights. We also show data from ground-based Sun/sky radiometers, from a ground-based lidar, and from a downward-pointing lidar aboard the high-flying NASA ER-2 aircraft for all cases where a comparison between one of these instruments and AATS-14 is possible. Finally, we show all comparisons of $\tau_a(\lambda)$ as measured by AATS-14 and retrieved over water and over land by four different spaceborne instruments (TOMS, MODIS, MISR and ATSR-2).

2. Measurements

2.1. Airborne Measurements

2.1.1 The NASA Ames Airborne Tracking 14-channel Sunphotometer (AATS-14)

The AATS-14 measures the transmission of the direct solar beam in 14 spectral channels (0.354 to 1.557 μm). Azimuth and elevation motors controlled by tracking-error signals derived from a quad-cell photodiode rotate a tracking head to lock on to the solar beam and keep detectors normal to it. The tracking head is mounted outside the aircraft skin to minimize blockage by aircraft structures and to avoid data contamination by aircraft-window effects. Window defogging is achieved by a foil heater. Each channel consists of a baffled entrance path, interference filter, photodiode detector, and integral preamplifier. The filter/detector/preamp sets are temperature controlled to avoid thermally induced calibration changes.

The AATS-14 is designed to operate on a variety of aircraft, some of which may be remotely piloted. It can locate and track the sun without input from an operator and record data in a self-contained data system. In addition, it must interface to an aircraft-provided data system, and receive and execute commands from a remote operator station (laptop), and transmit science and instrument-status data to that station. Using aircraft-provided data on latitude, longitude and ambient static pressure, $\tau_a(\lambda)$ and CWV are computed in real-time and displayed at the operator station (along with raw data, instrument status, and aircraft-provided data). Radiometric calibration is determined via Langley plots [*Schmid and Wehrli*, 1995], either at high-mountain observatories or during specially designed flights [*Schmid et al.,* 2000].

The AATS-14 made its first science flights on the Pelican (modified Cessna) aircraft of the Center for Interdisciplinary Remotely Piloted Aircraft Studies (CIRPAS) during the Tropospheric Aerosol Radiative Forcing Observational Experiment (TARFOX) in July 1996 [*Russell et al.,* 1999a,b]. More extensive flights on the Pelican were made in the second Aerosol Characterization Experiment (ACE-2), which provided many measurements of marine, European, and African aerosol optical depth spectra, as well as water vapor columns [*Schmid et al.,* 2000].

Our methods for data reduction, calibration, and error analysis have been described previously [*Russell et al*., 1993; *Schmid and Wehrli*, 1995; *Schmid et al*., 1998 and 2001]. A brief summary is given here. The AATS-14 channels are chosen to allow separation of aerosol, water vapor, and ozone transmission. From these slant-path transmissions we retrieve $\tau_a(\lambda)$ in 13 narrow wavelength bands and the columnar amounts of water vapor (CWV) and ozone. Due to large transmission loss of the 0.605-μm bandpass filter (the AATS-14 channel most sensitive to ozone) and hence large calibration uncertainty, the ozone retrieval was turned off for the results

shown here and the total column ozone values were taken from the Total Ozone Mapping Spectrometer (TOMS) on the Earth Probe satellite. In addition to the corrections for Rayleigh scattering and O_3 absorption, some channels require corrections for NO_2, H_2O and O_2-O_2 absorption. Most cross-sections were computed using LBLRTM 5.21 [*Clough, and Iacono*, 1995] using the ESA-WV H_2O line-list of *Schermaul et al*. [2001]. NO_2 and O_2-O_2 cross-sections not included in LBLRTM 5.21 were taken from *Harder et al*. [1997], *Schneider et al.* [1987], *Greenblatt et al*. [1990] and *Michalsky et al*., [1999]. NO_2 was assumed constant at 2×10^{-15} molecules cm^{-2}.

During SAFARI 2000, AATS-14 acquired data of good quality during 24 data flights. Unlike in ACE-2 [*Schmid et al.,* 2000] we did not perform in-flight Langley plots during SAFARI 2000. Instead, AATS-14 was calibrated at the Mauna Loa Observatory, Hawaii, three months before and one month after the SAFARI 2000 campaign using the Langley plot technique [*Schmid and Wehrli*, 1995]. As a result of band-pass filter degradation, the calibration constants obtained from the post-mission calibration were lower than those obtained from the pre-mission calibration. However, for seven of the 14 wavelengths the change was only 0.5% or less. Six of the other seven channels had degraded by 1 to 6% and one filter lost 11% of its transmission. We decided to discard the results from the last mentioned filter. Thus, the SAFARI 2000 data set consists of 12 wavelengths (0.354, 0.380, 0.449, 0.499, 0.525, 0.606, 0.675, 0.778, 0.864, 1.019, 1.241, and 1.557 μm) at which we retrieve τ_a and the 0.940-μm wavelength, which we use to determine CWV. Note that

$$\Delta\tau_a(\lambda) = \frac{1}{m}\frac{\Delta V_0(\lambda)}{V_0(\lambda)} \tag{1}$$

with

$$m \approx \frac{1}{\cos\theta} \tag{2}$$

Hence a relative uncertainty of 1% in the calibration constant V_0 will lead to an absolute uncertainty in the aerosol optical depth $\Delta\tau_a(\lambda)$ of 0.01 for a solar zenith angle $\theta = 0°$. To determine the most plausible set of calibration constants applicable to the SAFARI 2000 data set we inspected $\tau_a(\lambda)$ spectra measured during higher altitude legs (typically around 4 km). We focused on days with low τ_a (0.007 to 0.04 at 0.499 μm, at around 4 km). This resulted in 13 spectra taken during 11 flights between August 14 and 31, 2000. The cleanest conditions were observed early in the campaign before the onset of intense biomass burning [*Annegarn et al*., this issue]. Leaving the calibration constants of the seven stable channels unchanged we then adjusted the calibration constants of the other five aerosol wavelengths in such a fashion that the retrieved $\tau_a(\lambda)$ yielded "smooth" $\tau_a(\lambda)$ spectra for all 13 high-altitude cases. In all but one channel the adjusted calibration constants were within the bounds of pre- and post-mission calibration.

The total uncertainty of the retrieved $\tau_a(\lambda)$, due to uncertainties in calibration, sun-tracking, signal measurement, airmass computation, and corrections of molecular scattering and absorption, was computed following the procedures given by *Russell et al.* [1993]. The uncertainty in CWV was computed following *Schmid et al.* [1996]. During SAFARI 2000, AATS-14 data were recorded every 4 seconds consisting of an average of 9 samples taken in the first 3 of the 4 seconds. The sample standard deviation of all science detector outputs is also stored in the data files. These standard deviations were used in our cloud-screening algorithm that is based on clouds exhibiting higher standard deviations than clear sky.

2.1.2 The Cloud Physics Lidar (CPL)

The Cloud Physics Lidar (CPL) was built for use on the NASA ER-2 high altitude aircraft. Its purpose is to provide multi-wavelength (0.355 μm, 0.532 μm, and 1.064 μm) measurements of cirrus, sub-visual cirrus, and aerosols with high temporal and spatial resolution. This instrument together with initial SAFARI 2000 measurement results has been described by *McGill et al*., [2002].

The CPL is the successor of the Cloud Lidar System (CLS), which was the first high altitude lidar system designed specifically for studying clouds and aerosols and was first flown on the ER-2 aircraft in 1983. The first deployment of the CPL was the SAFARI 2000 field campaign. Pointing downward from the ER-2 operational altitude of ~20 km, CPL obtained 120 flight hours of data with no problems or failures. The results are discussed by *McGill et al.*, [this issue].

In this paper we use aerosol extinction $E_a(\lambda)$ and $\tau_a(\lambda)$ profiles at 0.532 and 1.064 μm obtained from CPL in five ER-2 flights (the 0.355-μm channel was not yet operational during SAFARI 2000). The CPL data segments were chosen to coincide temporally and spatially with Convair-580 vertical profiles to allow comparisons with AATS-14 measurements.

2.2 Ground-based measurements

2.2.1 Aerosol Robotic Network (AERONET)

AERONET is a globally dispersed network of automatic ground-based Sun/sky scanning radiometers from which $\tau_a(\lambda)$, CWV, aerosol size distribution and aerosol single-scattering albedo, ω_0, are retrieved [*Holben et al*., 1998 and 2001; *Eck et al*., 2001; *Dubovik et al*., 2002]. Seventeen southern-African AERONET sites were operational during SAFARI 2000. Detailed results are presented by *Eck et al*. [this issue]. Here we present data from seven AERONET sites

(Table 1) coincident with Convair-580 low-altitude fly-by's, thereby allowing comparisons with AATS-14 airborne measurements and satellite sensors.

2.2.2 Micro-Pulse Lidar Network (MPL-Net)

The Micro-Pulse Lidar (MPL) [*Spinhirne et al*., 1995] is a single channel (0.523 μm), autonomous, eye-safe lidar system originally developed at the NASA Goddard Space Flight Center and is now commercially available. MPL-Net [*Welton et al*., 2002] is a worldwide network of ground-based MPL systems, co-located with AERONET Sun/sky radiometers. The MPL is used to determine the vertical structure of clouds and aerosols. The MPL data is analyzed to produce optical properties, such as extinction and optical depth profiles of clouds and aerosols.

During SAFARI 2000, MPL systems were deployed at Skukuza in the Kruger National Park, South Africa, and in Mongu, Zambia (Figure 1 and Table 1). Detailed results are presented by *Campbell et al*. [this issue]. Several times during the campaign the ER-2 overflew the MPL sites to allow comparison with the airborne CPL. The Convair-580 flew one vertical profile over each MPL site to permit comparison with airborne AATS-14 measurements.

2.3 Spaceborne measurements

A major focus of the SAFARI 2000 dry season campaign was validation of satellite retrieved aerosol properties. Mostly, these validations are accomplished using ground-based AERONET data [e.g., *Diner et al*., 2001; *Chu et al*., 2002; *Remer et al.*, 2002; *Torres et al*., 2002; *Zhao et al.*, 2002]. Airborne sensors (such as AATS-14 and CPL) have less temporal coverage but they can provide aerosol optical properties over water, in vertical profiles, and along aerosol gradients. They can also help address the problem of small-scale, sub-pixel variability.

During SAFARI 2000, ER-2 and Convair-580 flights were coordinated with overpasses of the Terra and, to a lesser extent, with the Earth Probe satellite.

2.3.1 Total Ozone Mapping Spectrometer (TOMS)

TOMS radiation measurements at two near-UV channels are used to retrieve aerosol optical depth and single scattering albedo [*Torres et al*., 1998]. The retrieval technique applied to the TOMS data makes use of two advantages of near-UV remote sensing not available in the visible or near IR: 1) low reflectivity of all land surface types (including deserts, which are normally bright in the visible), enabling aerosol retrieval over the continents, and, 2) high sensitivity to aerosol types that absorb in the UV, allowing clear separation between carbonaceous and mineral aerosols from purely scattering particles such as sulfate and sea salt aerosols.

The near-UV method of aerosol characterization has been validated by comparison with AERONET ground based observations [*Torres et al*., 2002]. The predicted uncertainty of TOMS retrieved τ_a at 0.38 μm is the larger of 0.1 and 20% of τ_a for non-absorbing aerosols and the larger of 0.1 and 30% of τ_a for absorbing aerosols. *Torres* et al. (2002) performed 496 individual comparisons with six AERONET sites and found 74% of all τ_a to agree within the predicted uncertainties. A long-term record of τ_a over oceans and continents has been derived using observations of backscattered near ultraviolet radiation from the TOMS sensors on board the Nimbus-7 (1979-1992) and the Earth-Probe (mid-1996 to present) satellites [*Torres et al*., 2002].

During SAFARI 2000, several Convair-580 flights were coordinated with overpasses of the Earth Probe satellite allowing comparisons of TOMS aerosol retrievals with AATS-14 column and profile measurements.

2.3.2 Moderate Resolution Imaging Spectroradiometer (MODIS)

"Aerosol physical parameters are among the numerous products operationally retrieved from the Moderate Resolution Imaging Spectroradiometer (MODIS) onboard the Earth Observing System's (EOS) Terra satellite launched on 18 December 1999. The MODIS aerosol algorithm routinely retrieves $\tau_a(\lambda)$ at 0.47 and 0.66 μm wavelengths (and interpolates to 0.55 μm) over vegetated land surfaces, and at seven spectral bands (0.47, 0.55, 0.66, 0.87, 1.24, 1.64 and 2.13 μm) over oceans [*Kaufman et al*., 1997; *Tanré et al*., 1997]. Other aerosol parameters retrieved include the Angstrom exponent over land and ocean, and effective radius and ratio of small to large particle size modes over ocean." (from *Ichoku et al*. [2002])

The MODIS aerosol retrievals over ocean and land have been validated by comparison with AERONET ground based observations. For the over-ocean retrievals, *Remer et al*. [2002] performed 64 individual comparisons with data from 11 coastal and island AERONET stations covering a time span of 2 months starting August 21, 2000. They found MODIS retrieved τ_a at 0.66 μm and 0.87 μm to agree within the expected uncertainty $\Delta\tau_a = \pm 0.03 \pm 0.05\tau_a$.

To validate the over-land $\tau_a(\lambda)$ retrieval, *Chu et al.* [2002] performed 315 individual comparisons with 32 AERONET land sites covering the period from July to September 2000. They found that nearly all points (at 0.47 μm and 0.66 μm) fell within the retrieval errors of $\Delta\tau_a = \pm 0.05 \pm 0.2\tau_a$.

During SAFARI 2000, numerous Convair-580 flights were coordinated with overpasses of the Terra satellite allowing comparisons of MODIS aerosol retrievals with AATS-14 column and profile measurements.

2.3.3 Multi-angle Imaging SpectroRadiometer (MISR)

The MISR, also onboard the Terra satellite, images the Earth at nine discrete view angles from nadir up to 70.5° fore and aft of the local vertical. Multi-spectral (0.446, 0.558, 0.672 and 0.866 μm) imagery is obtained at each angle. MISR globally provides 275-m sampling in all bands of the nadir camera and the red band of each of the off-nadir cameras and 1.1 km for the remaining cameras. It takes 7 minutes for all nine cameras to image a given location. Aerosol optical properties over land and water are retrieved over 17.6×17.6 km^2 regions. The aerosol retrieval algorithm has been described by *Martonchik et al.* [1998] and *Kahn et al*. [2001]. A first validation of the over-land retrieval using SAFARI 2000 AERONET data has been discussed by *Diner et al*. [2001].

2.3.4 Along Track Scanning Radiometer 2 (ATSR-2)

The ATSR-2 is a radiometer aboard the European ERS-2 satellite, which was launched in April 1995. ATSR-2 has seven spectral bands; four of these are potentially useful for aerosol retrieval. The effective wavelengths of these four channels are 0.555, 0.659, 0.865 and 1.6 μm. The spatial resolution is approximately 1×1 km^2 at nadir. The swath width is 500 km. The ATSR-2 has a conical scanning mechanism, thus producing two views of each region: first a forward view (zenith angle approximately 55°) and about two minutes later a nadir view. Validations of the over-water and the over-land τ_a retrievals using AERONET and also airborne sunphotometer data have been presented by *Veefkind et al*. [1998, 1999] and *Robles-Gonzalez et al.* [2000].

No flight coordination with ATSR-2 overpasses was made during SAFARI 2000, but we present one comparison of opportunity below.

3. Results

All locations for which we discuss results are shown in the map in Figure 1. From August 10 to September 9 the Convair-580 was based in Pietersburg, South Africa for the purpose of carrying out flights over South Africa, Botswana, Zambia and Mozambique. From September 10 to 18, the Convair-580 was based in Walvis Bay, Namibia to carry out flights over Namibia and off the Namibian coast [*Hobbs*, this issue a].

3.1. Comparing $\tau_a(\lambda)$ obtained from AATS-14 and AERONET

As shown in Table 1, the Convair-580 made eleven low-altitude fly-by's of seven AERONET sites, allowing comparison of $\tau_a(\lambda)$ derived from the airborne AATS-14 and the ground-based Sun/sky radiometers measurements. The low-altitude AATS-14 $\tau_a(\lambda)$, consisting of 4 to 54 sec averages, were usually compared to the AERONET $\tau_a(\lambda)$ closest to the overflight time. In one case we linearly interpolated the AERONET $\tau_a(\lambda)$ to the exact AATS-14 time, because there was a considerable change in the AERONET observed $\tau_a(\lambda)$. Note that except at low sun angles AERONET measures $\tau_a(\lambda)$ every 15 min. Due to safety considerations and competing mission objectives, the vertical (-66 to 279 m) and/or horizontal separation (2 to 45 km) between the airplane and AERONET sites was not always optimal. Note that in cases where there is a horizontal separation it is possible for the Convair-580 to fly below the AERONET site altitude. For this and also for the subsequent comparisons with satellite results we have made no correction for aerosol extinction below the lowest altitude of the airplane.

The results of the intercomparison are shown in Figure 2 and Figure 3. With the exception of the Sua Pan location, all AERONET Sun/sky radiometers operated at 0.34, 0.38, 0.44, 0.5, 0.67, 0.87, and 1.02 μm wavelengths. In the scatter plots in Figure 2 we directly compared the

AERONET and AATS-14 τ_a at 0.38/0.38, 0.5/0.499, 0.67/0.675, 0.87/0.864, and 1.02/1.019 μm without any adjustments for the slight differences in wavelength. However, we inter/extrapolated the AATS-14 $\tau_a(\lambda)$ to the 0.34 and 0.44 μm AERONET wavelengths using the equation

$$\ln \tau_a(\lambda) = a_0 + a_1 \ln\lambda + a_2 (\ln\lambda)^2 \quad (3)$$

where the constants a_0, a_1, and a_2 are determined by a second-order polynomial fit to each individual AATS-14 $\tau_a(\lambda)$ spectrum. An excellent discussion of (3), applied to a variety of aerosol types is given by *Eck et al*. [1999]. As can be seen in Figure 3, eqn. (3) provides a good representation of the measured $\tau_a(\lambda)$. Subplots k) and l) in Figure 3 show the effect of dirt on the AATS-14 optical window affecting the longest two wavelengths. It is typical for AATS-14 that if the optical window picks up dirt after flying through a cloud or through sea spray, then this tends to happen first in the two longest wavelengths channels since their position is behind the uppermost section of the window which protrudes most above the aircraft skin. The statistical comparison shown in Figure 2 results in rms differences ranging from 0.023 to 0.075 (6 to 15%) and regression line slopes between 0.9 and 1

Schmid et al. [1999] compared τ_a derived from four ground-based solar radiometers (one was an AERONET Sun/sky radiometer and one was AATS-6, an abbreviated version of AATS-14) operated at the same site during a 3-week field campaign in Oklahoma. They found that the τ_a values from 0.38 to 1.02 μm agreed to within 0.015 (rms). The somewhat larger absolute rms differences (0.023 to 0.075) found in the fly-by comparisons shown here are a result of spatial (vertical and horizontal) and temporal separations, the effects of dirt on the AATS-14 optical window, tracking imperfections of AATS-14, the larger number of individual instruments involved, and most importantly, larger τ_a in SAFARI 2000 than in *Schmid et al*. [1999]. In fact

the relative differences (rms/$\tau_a(\lambda)$) for the comparison between the AERONET Cimel and AATS-6 in *Schmid et al*. [1999], were 7%, 6%, 12%, 18% and 12% at 0.380, 0.450, 0.525, 0.864, and 1.021 μm, respectively, and thus comparable to the relative differences found in SAFARI 2000 (Figure 2) with the fly-by comparisons.

3.2. AATS-14 measurements of a biomass burning smoke plume: a case study

Smoke from biomass burning was a major component of the Southern African aerosol during SAFARI 2000. Thus, significant portions of the Convair-580 flight hours were devoted to studying smoke from prescribed fires and fires of opportunity (see *Hobbs*, this issue a and references therein).

Here we discuss airborne $\tau_a(\lambda)$ measurements of smoke originating from a flaming hot grass-fire on August 17, 2000 in the Kruger National Park north of Skukuza (24°28'S/31°50'E). Between 11:05 and 11:31 UT the Convair-580 penetrated the smoke plume four times at a near constant flight altitude of 1100 m (113 m a.g.l.). Figure 4 shows the time traces of $\tau_a(\lambda)$ obtained from the four consecutive penetrations. Measurement gaps in time traces are caused by temporary loss of sun-tracking after blockage of the sun by aircraft structures. Due to an AATS-14 tracking-software glitch (discovered and fixed after SAFARI 2000), any temporary obstruction of the solar beam hitting the sun-sensor caused the instrument to lock at its current position for 10 sec before re-acquiring the sun.

The atmosphere outside the plume was exceptionally clear with $\tau_a(\lambda)$ <0.1 at all wavelengths, whereas inside the plume $\tau_a(\lambda)$ occasionally exceeds 6 in the ultra-violet. The flight pattern flown in and outside the plume allowed derivation of the τ_a map shown in Figure 5. The τ_a measurements were taken at each individual white dot along the white Convair-580 flight

track shown in Figure 5. A triangle-based linear interpolation was used to fill in τ_a values between the flight tracks. The map clearly reveals the position and the spatial extent (9×13 km with $\tau_a(0.5\ \mu m) > 0.5$) of the plume.

The spectral parameters α^* and γ shown in Figure 4 are obtained by applying (3) to each $\tau_a(\lambda)$ spectrum, where $\alpha^* = -a_1$ and $\gamma = -a_2$. In fact, (3) is an extension of the traditional Ångstrom law

$$\tau_a(\lambda) = \beta\lambda^{-\alpha} \tag{4}$$

where the wavelength exponent α is related to the aerosol size distribution (see e.g. *Schmid et al*. [1997]. Typically $\sim 0 < \alpha < 1$ is found for larger particles and $1 < \alpha \leq \sim 2$ for smaller particles. However, we often find (4) to be a poor representation of $\tau_a(\lambda)$, as did *Eck et al*. [1999]. Hence, we prefer to use (3), which was also used by *Eck et al*. [1999], where α^* is still related to aerosol size and γ describes the curvature of the spectrum (in log-log space) or deviations from (4). Of course, if $\gamma = 0$ then (3) reduces to (4) and $\alpha^* = \alpha$.

The time traces of the spectral parameters in Figure 4 indicate rather flat slightly curved spectra ($\alpha^* \cong 0.5$, $\gamma \cong -0.75$) outside the plume, suggesting the presence of larger particles there, whereas, inside the plume the spectra are very steep with almost no curvature ($\alpha^* \cong 2$ to 2.5, $\gamma \cong 0$) indicating the dominance of small particles.

Figure 6a shows $\tau_a(\lambda)$ measured inside the smoke plume (average of fourth penetration) and outside the smoke plume (from 11:21-11:24 UT, south of the plume). Also shown in Figure 6a is the difference between the two $\tau_a(\lambda)$ spectra. The difference spectrum can be interpreted as the $\tau_a(\lambda)$ spectrum of the smoke alone. The aerosol size distributions can be estimated by inverting the $\tau_a(\lambda)$ spectra using the constrained linear inversion method of *King et al.* [1978] (see also

King [1982]; *Gonzàlez Jorge and Ogren* [1996]). In its present formulation, the inversion assumes an aerosol consisting of homogeneous spherical particles that are nondispersive (i.e. refractive index m independent of wavelength or size) over the wavelength range of the observations. For the inversion, we used m=1.51-0.021i determined from AERONET Sun/sky radiometers for African Savanna biomass burning aerosol [*Dubovik et al*., 2002]. Figure 6b shows the area size distributions inverted from the $\tau_a(\lambda)$ spectra in Figure 6a. Three inversion results are shown per case obtained by using three different initial estimates of the size distribution [*King et al*., 1978, *Schmid et al.*, 1997]. The solid lines in Figure 6a are $\tau_a(\lambda)$ spectra computed from the size distributions in Figure 6b. All size distributions exhibit a fine particle mode, but the fine mode is drastically enhanced in the in-plume and plume-only surface area distributions. The size distribution outside the plume appears bi-modal revealing also a coarse mode possibly caused by soil dust. This coarse mode may also be present in the smoke size distributions, but the inversion cannot retrieve it because its contribution to $\tau_a(\lambda)$ is negligible.

3.3. AATS-14 vertical profiles

When the Convair-580 flew vertical profiles, AATS-14 could be used to measure vertical profiles of $\tau_a(\lambda)$ and CWV. Differentiation of these profiles leads to spectral aerosol extinction $E_a(\lambda)$ and water vapor density (ρ_w) profiles [*Schmid et al*., 2000]. In Figure 7, we show nine examples of AATS-14 vertical profiles obtained during SAFARI 2000. To facilitate comparisons we plotted all profiles on the same scale. Occasionally $\tau_a(\lambda)$ or CWV decreased (increased) when the plane descended (ascended). In a horizontally homogeneous, time-invariant atmosphere, this would be impossible. However, in the real atmosphere it can occur because (1) the sunphotometer can only measure the transmittance of the sunphotometer-to-sun path, (2) that path in general passes through a horizontally inhomogeneous, time-varying atmosphere, and (3)

the path and the atmosphere move with respect to each other as the aircraft moves and the wind blows. Before the sunphotometer $\tau_a(\lambda)$ or the CWV profile is vertically differentiated to obtain $E_a(\lambda)$ or ρ_w, it has to be smoothed (in a non-biased manner) to eliminate increases in $\tau_a(\lambda)$ or CWV with height. In this study, smoothed spline fits (dashed lines in Figure 7) were used for this purpose. However, to avoid over-smoothing at altitudes that exhibit actual variations of $\tau_a(\lambda)$ we occasionally allow $E_a(\lambda)$ or ρ_w to become slightly negative.

The profiles for Skukuza (Aug 22), Inhaca Island (Aug 24), Beria (Aug 31) and Maun (Sep 2) show aerosol layers with $E_a(0.5\ \mu m)$ around 0.15 km^{-1}, with most or all of the aerosol below the highest flight altitude. The profiles for Sua Pan (Sep 3) and Mongu (Sep 6) show massive thick aerosol layers extending above the maximum flight altitude, with E_a (0.5 μm) as large as 0.35 km^{-1}. In contrast, the profile over Phalaborwa (Sep 7) shows a very clean situation with virtually the entire aerosol confined to altitudes below 3.5 km. The profiles off the Namibian Coast (Sep 13) and over Etosha National Park (Sep 16) show elevated aerosol layers extending above the maximum flight altitude. Layers of remarkably low extinction between heavily polluted air were a common feature during SAFARI 2000. Examples can be seen on Aug 24, Sep 7 and Sep 13. *Hobbs* [2002 and this issue b] studies these layers - which he refers to as "clean air slots" - using Convair-580 in-situ aerosol measurements. Figure 7 shows that the clean air slots coincide with local minima of ρ_w. The CWV and ρ_w profiles reach high values only if the profiles extend to low altitudes above sea level. In the cases where the aerosol extends above the maximum flight altitude the same behavior is observed for the water vapor. We also applied (3) to each of the $\tau_a(\lambda)$ and $E_a(\lambda)$ spectra shown in Figure 7. The spectral parameters α^* and γ obtained from $\tau_a(\lambda)$ are indicative of the particle size distribution of the atmospheric column above the aircraft, whereas, α^* and γ obtained from $E_a(\lambda)$ describe the local size distribution. For

virtually all of the profiles we found $\alpha^* \cong 2$ and $\gamma \cong 0$ (obtained from $E_a(\lambda)$) indicative of small biomass burning aerosol. Exceptions are Skukuza (Aug 22) with $\alpha^* \cong 1.5$ (larger particles mixed in), Phalaborwa with $\alpha^* \cong 1$ (clean, no biomass burning aerosols) and Inhaca Island where α^* decreased towards 0 at lower altitudes (effect of larger sea salt particles).

3.4. AATS-14 aerosol vertical profiles compared with lidar measurements (MPL and CPL)

The accuracies of the vertical profiles of $\tau_a(\lambda)$ and CWV measured with AATS-14 depend on the measurement errors discussed earlier, but the accuracies are also limited by the horizontal inhomogeneity and time-variance of the atmosphere. While all time-independent measurement errors in $\tau_a(\lambda)$ or CWV cancel out when the profiles are differentiated, horizontal inhomogeneity and time-variance of the atmosphere have significant impact on the $E_a(\lambda)$ and ρ_w profiles. The advantage of an airborne sunphotometer is that the measured $\tau_a(\lambda)$ and $E_a(\lambda)$ represent the ambient aerosol unperturbed by sampling effects, yet they can be matched in space and time to in-situ measurements made on the same aircraft. In a companion paper, *Magi et al*. [this issue] compare AATS-14 layer $\tau_a(\lambda)$ and $\tau_a(\lambda)$ profiles with Convair-580 in-situ aerosol measurements. Here we compare the $\tau_a(\lambda)$ and $E_a(\lambda)$ profiles obtained from AATS-14 with the ground based MPL at Skukuza and with the CPL instrument aboard the ER-2.

Good flight plan coordination between the ER-2 and Convair-580 (i.e. the Convair-580 flying a vertical profile with the ER-2 passing over the same area) led to five aerosol vertical profile comparisons between CPL on the ER-2 and AATS-14. One of the comparisons was carried out over the Skukuza MPL site and another one over the Mongu MPL site. Due to an operator error, the Mongu MPL data was not stored on the day of the comparison.

Figure 8 shows the comparison over Skukuza on August 22. The AATS-14 $\tau_a(\lambda)$ are identical to those shown in Figure 7, but only the wavelengths most closely matching the lidar wavelengths are shown. The CPL and MPL inversions used an altitude-independent backscatter-to-extinction ratio, S_a, constrained so that the height integral of each lidar extinction profile matches the corresponding $\tau_a(\lambda)$ observed simultaneously by the Skukuza AERONET Sun/sky radiometer. As shown in Figure 3c, the $\tau_a(\lambda)$ spectrum measured by AATS-14 at the lowest Convair-580 flight altitude agrees well with AERONET. Therefore, as expected the $\tau_a(\lambda)$ profiles agrees well near the ground. However, the agreement among all three instruments is remarkable throughout the entire profile ($\tau_a(\lambda)$ and $E_a(\lambda)$). Adjusting the CPL results from 0.532 μm to 0.525 μm would further increase the agreement. All instruments show strong capping near 3.2 km, and the lidars indicate a second aerosol layer topping out at 4.5 km (above the Convair-580 profile top). The resulting S_a values are 66 sr for the MPL (0.523 μm) and 60.5 sr and 36 sr for the CPL at 0.532 μm and 1.064 μm, respectively.

Figure 9 shows the comparison over Inhaca Island on August 24. The AATS-14 $\tau_a(\lambda)$ profile at all wavelengths is shown in Figure 7, but for the comparison in Figure 9 we interpolated the AATS-14 $\tau_a(\lambda)$ and $E_a(\lambda)$ to the CPL wavelengths using Eq. (1). The inversion of the CPL data was constrained so that the integrated extinction profiles return the $\tau_a(\lambda)$ observed simultaneously by the Inhaca AERONET Sun/sky radiometer. This resulted in S_a values of 46.7 sr and 27.9 sr at 0.532 μm and 1.064 μm, respectively. As shown in Figure 3d, the $\tau_a(\lambda)$ measured by AATS-14 at the lowest Convair-580 flight altitude agree well with AERONET in the UV and visible but not in the near-IR. Consequently, the CPL and AATS-14 $\tau_a(\lambda)$ profiles near the ground agree well at 0.532 μm but not at 1.064 μm. However, the 0.532 μm AATS-14 τ_a is offset from the CPL τ_a for most of the profile. The $E_a(\lambda)$ profiles match closely above 1 km,

but below that altitude, the AATS-14 $E_a(\lambda)$ profile exhibits an unrealistic behavior. Both instruments nicely show the clean air slot near 3 km. The CPL shows a third weak aerosol layer centered at 7 km (above the Convair-580 profile top).

Figure 10 shows the comparison over Senanga on September 6. The inversion of the CPL data was constrained to match the $\tau_a(\lambda)$ observed simultaneously at the Senanga AERONET site (S_a=72.2 sr and 32.2 sr). As shown in Figure 3g, the $\tau_a(\lambda)$ measured by AATS-14 are slightly less than the AERONET results, which we attribute to the fact that the lowest Convair-580 flight altitude was 150 m above ground level. The CPL and AATS-14 $\tau_a(\lambda)$ and $E_a(\lambda)$ agree well in general but with larger differences at the 0.532 μm wavelength near the ground. The CPL shows the massive, thick aerosol layer topping out near 5.8 km a.s.l.

The shaded area depicts the altitude above sea level of the underlying terrain.

Figure 11 shows the comparison over Mongu also on September 6. The inversion of the CPL data was constrained to match the $\tau_a(\lambda)$ observed simultaneously at the Mongu AERONET site (S_a=70.5 sr and 33.7 sr). As shown in Figure 3h, the $\tau_a(\lambda)$ measured by AATS-14 agrees well with the Sun/sky radiometer when flying 30 m above ground near the AERONET site, but are slightly lower when flying 120 m above the AERONET instrument (Figure 3i). The CPL and AATS-14 $\tau_a(\lambda)$ and $E_a(\lambda)$ profiles agree reasonably well at all altitudes. The CPL shows the massive, thick aerosol layer extending to 6 km a.s.l.

Figure 12 shows the comparison over water off the Namibian Coast on September 11. Since there was not an AERONET site the inversion of the CPL data was constrained to match the AATS-14 $\tau_a(\lambda)$ observed at the lowest Convair-580 flight altitude (S_a=79.9 sr and 38.8 sr). The CPL and AATS-14 $\tau_a(\lambda)$ and $E_a(\lambda)$ profiles agree very well at almost all altitudes. CPL shows

the aerosol layer extending downward from 6 km altitude with a strong maximum near 5.3 km, and a nearly continuous decrease in extinction until ~600 m where the lidar beam hits a low cloud with no returns from below the cloud. The AATS-14 measurements obtained after completion of the vertical profile confirm the existence of the cloud. The spectral parameters α^* and γ indicate the dominance of small particles throughout the profile especially above 2.5 km. This suggests that the elevated aerosol layer consists of biomass burning aerosol advected off the continent, whereas, most of the marine boundary layer aerosol is masked by the presence of the low cloud.

3.5. TOMS τ_a comparison

During SAFARI 2000, several Convair-580 flights were coordinated with overpasses of the Earth Probe satellite. This resulted in three successful match-ups where the TOMS aerosol retrievals can be compared with AATS-14 column and profile measurements. Figure 13 shows the TOMS retrieved τ_a at 0.38 μm compared to $\tau_a(\lambda)$ obtained from AATS-14 during low altitude passes performed within or near a TOMS pixel.

On Sep 2, 2000 the Convair-580 flew a downward spiral, followed by a low-altitude horizontal leg over the instrumented tower at Maun, Botswana. This entire flight segment lasting from 9:53 until 10:12 UT was located within one 40×40 km^2 TOMS pixel acquired at 9:48 UT. Figure 13a shows the $\tau_a(\lambda)$ comparison obtained during the low-altitude leg. The agreement is within the TOMS predicted error bar for absorbing aerosols. The AATS-14 vertical profile obtained during the downward spiral is shown in Figure 7. The extinction at 0.5 μm wavelength increases gradually from 0 km^{-1} at 4.3 km to 0.22 km^{-1} near the surface. It should be noted that the TOMS retrieval algorithm for absorbing aerosols assumes that the UV-absorbing aerosols are

concentrated in a single layer represented by a Gaussian distribution centered at 2.9 km above sea level. Throughout the entire AATS-14 $E_a(\lambda)$ profile we find $\alpha^* \cong 2$ and $\gamma \cong 0$ indicating the dominance of small particles (likely from biomass burning), which is consistent with the fact that TOMS retrieved an absorbing aerosol with $\omega_0(0.38\ \mu m)=0.925$.

On Sep 6, 2000 the Convair-580 flew several vertical profiles and low-altitude legs near Mongu Zambia. The AATS-14 $\tau_a(\lambda)$ obtained during a low altitude leg and $\tau_a(\lambda)$ obtained from the Maun AERONET site were located within the same TOMS pixel acquired at 10:07 UT. The τ_a agreement (Figure 13b) is again within the TOMS predicted error bar for absorbing aerosols. Most of the AATS-14 vertical profile shown in Figure 7 is also contained in that same TOMS pixel. From the $E_a(\lambda)$ profile we find $\alpha^* \cong 2$ to 2.4 $\gamma \cong 0$ to 0.6 indicating an even stronger dominance by small particles. In accordance with that, TOMS retrieved a strongly absorbing aerosol with $\omega_0(0.38\ \mu m)=0.833$. However, the actual aerosol vertical profile (see The shaded area depicts the altitude above sea level of the underlying terrain.

Figure 11) is markedly different from the idealized profile assumed in the TOMS retrieval.

On Sep 7, 2000 the Convair-580 flew several low-altitude horizontal legs in and near a large prescribed fire in the Timbavati Game Reserve, South Africa. The prescribed fire was ignited around 8:20 UT. TOMS overpass time was one hour later. It is unlikely that the resulting smoke would fill an entire TOMS pixel only one hour after ignition. Hence, we decided to compare the cleanest AATS-14 low-altitude pass away from the fire with the closest TOMS pixel (Figure 13c). The AATS-14 total column $\tau_a(\lambda)$ spectrum is relatively flat ($\alpha^*=1.0$) indicating few if any small (smoke) particles. This is consistent with the fact that TOMS retrieved a non-absorbing aerosol ($\omega_0(0.38\ \mu m)=1$). However, the TOMS retrieved τ_a (0.065) was significantly smaller than the AATS-14 measurement (~0.3). The TOMS retrieval at another comparable close

location (23.8S, 30.75S) was 0.057, consistent with the previous one. This suggests that either the AATS-14 spectrum was still influenced by smoke or that TOMS underestimates $\tau_a(\lambda)$ in this situation.

3.6. MODIS $\tau_a(\lambda)$ Comparison

During SAFARI 2000, numerous Convair-580 flights were coordinated with overpasses of the Terra satellite [*Hobbs et al*., this issue a]. However, factors such as timing, surface brightness (MODIS requires dark surfaces such as water or vegetation), sunglint, and statistical validation criteria allowed for only two successful match-ups with AATS-14.

Figure 14 (top) shows an over-water comparison near Inhaca Island off the coast of Mozambique west of the city Maputo. The timing was almost perfect with Terra passing over at 8:16 UT, a surface based AERONET Sun/sky radiometer measurement at 8:22 UT and the Convair-580 carrying AATS-14 reaching a flight altitude of 170 m a.s.l. at a distance of 7 km from the AERONET site at 8:24 UT. The MODIS $\tau_a(\lambda)$, representing a 10×10 km^2 area, agrees with AERONET and AATS-14 at all wavelengths within the retrieval error. To our knowledge, this is the first validation of MODIS τ_a at the 1.24 and 1.64 μm wavelengths. The vertical profiles from AATS-14 and CPL obtained in the same area are shown in Figure 7 and Figure 9 and are discussed in sections 3.3 and 3.4.

An over-land comparison obtained near the Kaoma AERONET site in Zambia is shown in Figure 14 (bottom). Although separated by more than 30 km (see Table 1), the AERONET and AATS-14 results agree closely. The MODIS retrieved $\tau_a(\lambda)$ is considerably less, and the disagreement is larger than the retrieval error. The MODIS $\tau_a(\lambda)$ spectrum is also much steeper than the other two spectra.

This result is consistent with recent findings that the MODIS-derived aerosol optical depths in Zambia are consistently lower than AERONET. In the MODIS $\tau_a(\lambda)$ validation done by *Chu et al*. (2002) the southern African region was represented only by the permanent AERONET sites at Skukuza (in South Africa) and Mongu (in Zambia). Combining the results of these two sites in a plot of MODIS versus AERONET $\tau_a(\lambda)$, *Chu et al.* [2002] obtained a best-fit line slope of 0.90 and 0.92 at 0.47 and 0.66 μm, respectively. However, if the stations had been separated in the analysis the slopes would have been near 1 for Skukuza and 0.7 for Mongu (*Chu*, personal communication). Furthermore, [*Hao et al.*, 2002] find that $\tau_a(\lambda)$ measured with 38 hand-held sunphotometers (and intercompared with AERONET) in western Zambia between June 11 and Oct 6 exceed MODIS retrieved $\tau_a(\lambda)$ by more than 40%. Possible reasons for the difference are currently under investigation. Using AERONET measurements, *Eck et al*. [this issue] find that the aerosol properties measured in Zambia differ from those observed at Skukuza (South Africa).

3.7. MISR $\tau_a(\lambda)$ Comparison

Since MISR is a new type of instrument, validation is especially important for the first algorithms used to interpret the data. The AATS team is engaged in a continuing effort with the MISR team to help in the validation effort. This section reports part of that work.

Careful inspection of SAFARI 2000 AATS-14 total column $\tau_a(\lambda)$ data and MISR $\tau_a(\lambda)$ retrievals led to successful match-ups at three sites and dates. None of these match-ups coincides with the match-ups between MODIS and AATS-14 discussed above, although both instruments fly aboard the Terra satellite. (The two instruments do not always have overlapping coverage because MODIS has a much wider swath than MISR, whereas, most MISR cameras are glint-free in regions where the single-angle MODIS view is glint-contaminated.)

It is important to stress that all MISR $\tau_a(\lambda)$ retrievals shown in this paper come from the "beta" version of the standard retrieval, which is an early post launch, unvalidated version of the algorithm. This retrieval is based on a list of prescribed aerosol mixture models. Each mixture is tested in terms of how well it reproduces the MISR-measured path radiances [*Martonchik et al*., 1998; *Kahn et al.,* 2001]. In their comparison of MISR aerosol retrievals with AERONET observations, *Diner et al*. [2001] reported Regional Mean Optical Depth (RMOD) at the MISR standard wavelength of 0.558 μm. The RMOD is the average of the τ_a resulting from all aerosol mixture models that pass a certain goodness-of-fit threshold. Here we present $\tau_a(\lambda)$ at all four MISR wavelengths for the single best-fitting or second-best-fitting mixture.

Figure 15 shows the comparison of MISR retrieved best-fit $\tau_a(\lambda)$ with the Skukuza AERONET Sun/sky radiometer and with AATS-14 during a low altitude horizontal pass of the Convair-580 within one 17.6×17.6 km^2 MISR region on August 22, 2000. The agreement is very good at the two shorter MISR wavelengths, but MISR's $\tau_a(\lambda)$ exceed AATS-14 and AERONET values at the two longer wavelengths. Given the limited range of particle mixtures in the "beta"-version algorithm's climatology, the best-fitting MISR $\tau_a(\lambda)$ spectrum is too flat. This mixture is "Dusty Continental," containing 75% sulfate and 25% dust accumulation mode aerosol. Indeed, the AATS-14 $E_a(\lambda)$ profile over Skukuza yields $\alpha^* \cong 1.5$, indicating the presence of larger particles; by contrast, most of the profiles in Figure 7 seem to be dominated heavily by small biomass burning aerosols. This spectral $\tau_a(\lambda)$ comparison and others analyzed by the MISR team indicate that the "beta" version of the MISR algorithm does not contain enough small particles.

Figure 16 shows MISR data acquired over northwestern Botswana on September 3, 2000 (Terra Orbit 3786). The left image is a red, green, blue (RGB) composite of radiometrically calibrated, geo-located data from the nadir camera. The right image shows best-fit τ_a at 0.558

μm; the pixellation shows individual 17.6×17.6 km^2 regions. Because the MISR aerosol retrievals are also used for atmospheric correction of surface parameters, the "beta" version of the algorithm fills in the aerosol field with neighboring successful retrievals for regions where the aerosol retrieval fails, and labels the product accordingly. For this study, we use only regions that are not in this category. The bright features in the northwestern quadrant of the RGB picture are the dry lakebeds of the Makgadikgadi Pans. During SAFARI 2000, Sua Pan (marked in Figure 16) was the location of extensive ground-truth measurements made by M. Helmlinger et al. for MISR and AirMISR [*Diner et al*., 1998] validation [*Abdou et al*., this issue]. The suite of instruments used included an AERONET station (#59).

Figure 17 shows the comparison of MISR retrieved $\tau_a(\lambda)$ with the Sua Pan AERONET Sun/sky radiometer and with AATS-14 during a low altitude pass of the Convair-580 within two adjacent 17.6×17.6 km^2 MISR regions on September 3, 2000. The AERONET instrument was located in the 17.6×17.6 km^2 MISR region shown in the top plot, but the data are repeated in the bottom plot for reference purposes. The Convair-580 track actually crossed three adjacent MISR $\tau_a(\lambda)$ pixels but only the first two have successful aerosol retrievals.

From Figure 17 we see that for both pixels the "Clean Continental" mixture (95% sulfate and 5% black carbon) leads to good agreement at the 0.558-μm standard wavelength. The "Industrial Continental" mixture (90% sulfate and 10% black carbon) leads to higher $\tau_a(\lambda)$ values. Both spectra are too flat with respect to AERONET and AATS-14, but the Clean Continental is flatter. It is also evident from Figure 17 that $\tau_a(\lambda)$ does not change significantly when AATS-14 is flown from one MISR 17.6×17.6 km^2 region to the next one, because the agreement between AATS-14 and the stationary AERONET instrument remains. However, between the two regions the MISR algorithm switches best-fit mixtures, which leads to a change

in best-fit $\tau_a(\lambda)$. The "beta" version of the MISR algorithm contains only one small-sized component particle – black carbon (characteristic radius 0.012 microns). The smallest spherical, non-absorbing particle is sulfate, having a characteristic radius about seven times larger. Since smaller particles produce steeper slopes, the algorithm is forced to choose between small particles that are too dark, producing too high an optical depth, or lighter particles that are too large, giving too shallow a slope.

Figure 18 shows the comparison of MISR retrieved $\tau_a(\lambda)$ with AATS-14 during a low altitude pass of the Convair-580 within two adjacent 17.6×17.6 km^2 MISR regions off the Namibian Coast on September 11, 2000. In both regions, the "Clean Maritime" mixture (45% sulfate, 40% sea salt and 15% sea salt coarse) leads to good agreement at 0.558 μm and 0.672 μm; however, the MISR $\tau_a(\lambda)$ spectrum is again too flat. The "Industrial Maritime" mixture (70% sulfate, 10% sea salt, 20% black carbon) leads to a spectral slope agreeing with AATS-14 but the MISR $\tau_a(\lambda)$ values are then too high. As in the previous case, the MISR algorithm finds a different best-fit mixture in the two adjacent regions, leading to a large change in best-fit $\tau_a(\lambda)$, whereas, AATS-14 indicates very little change in $\tau_a(\lambda)$.

At the time of writing, the MISR team is in the process of revising the aerosol retrieval algorithm, based on a variety of validation and calibration tests, including those presented here, along with AERONET studies and MISR - AirMISR intercomparisons. The new algorithm's climatology has a finer size grid of spherical, non-absorbing aerosols, and includes smaller sizes.

3.8. ATSR-2 $\tau_a(\lambda)$ Comparison

A map of $\tau_a(0.555\ \mu m)$ from ATSR-2 aboard the ERS-2 satellite off the Namibian Coast on September 14, 2000 is shown in Figure 19. The red line marks the coastline. The white patches

show areas identified as clouds. The ATSR-2 map shows fairly clean conditions in general but increasing τ_a towards the coast.

On this same day, the Convair-580 carrying AATS-14 flew a low altitude horizontal leg just barely outside the ATSR-2 swath. The red filled circle in Figure 19 marks the approximate position of that leg. The distance to the closest pixels is less than 20 km, and the satellite overpass occurred 46 min before the aircraft leg. The comparison of ATSR-2 retrieved $\tau_a(\lambda)$ with AATS-14 during the low altitude leg is also shown in Figure 19. The wide AATS-14 error bars show measurement error, whereas, the narrow error bars show $\tau_a(\lambda)$ variability (2σ) in the low-altitude leg (3.4 km and 45 sec long, at height 95 m). The green dotted lines indicate the predicted uncertainty of ATSR-2 retrieved $\tau_a(\lambda)$ derived from comparison with various AERONET sunphotometers in Europe (*Robles-Gonzalez et al*., in preparation). The agreement is within error bars. AATS-14 shows a remarkably flat spectrum ($\alpha^*=0.13$) with no curvature. This slope is consistent with the ATSR-2 results.

The measurements were made over the ocean, and weather maps indicate along-shore flow; hence, the aerosol is expected to have a strong sea salt component. The observed offshore τ_a gradient is likely due to the decreasing influence of offshore advection of continental aerosol. The slightly higher ATSR-2 values as compared to the AATS-14 may result from this gradient.

4. Conclusions

During the dry season campaign of the Southern African Regional Science Initiative (SAFARI 2000) (August-September 2000), coordinated observations were made of massive, thick aerosol layers. Aerosol optical depth from λ=0.354 to 1.557 μm ($\tau_a(\lambda)$), columnar water vapor (CWV), and vertical profiles of aerosol extinction, ($E_a(\lambda)$), and water vapor density (ρ_w)

were obtained from the NASA Ames Airborne Tracking 14-channel Sunphotometer (AATS-14) aboard the University of Washington's Convair-580 research aircraft.

From August 10 to September 9 the Convair-580 was based in Pietersburg, South Africa, for the purpose of carrying out flights over South Africa, Botswana, Zambia and Mozambique. From September 10 to 18, the Convair-580 was based in Walvis Bay, Namibia, for flights over Namibia and off the Namibian coast. In this paper we have discussed a subset of the AATS-14 results from 24 data flights, and we have shown all valid comparisons with independent ground-based, airborne and space borne measurements.

The Convair-580 made eleven low-altitude fly-by's of seven AERONET sites, allowing comparison of $\tau_a(\lambda)$ derived from the AATS-14 and the ground-based Sun/sky radiometers measurements. The rms differences in $\tau_a(\lambda)$ ranged from 0.023 to 0.075 (6 to 15%). We presented a detailed study of an individual smoke plume from a grass fire, for which $\tau_a(\lambda)$ exceeded 6 in the ultra-violet. We have also presented and discussed vertical profiles of $\tau_a(\lambda)$, aerosol extinction, columnar water vapor, and water vapor density, for nine different locations and times. For virtually all of the profiles we found the spectral dependence of the aerosol optical depths indicated the dominance of small particles, presumably from biomass burning.

Excellent coordination between the high-flying ER-2 and the Convair-580 aircraft, with the Convair-580 flying vertical profiles as the ER-2 passed overhead, led to five aerosol vertical profile comparisons between the downward-pointing Cloud Physics Lidar CPL on the ER-2 and the AATS-14. One of the comparisons was carried out over a ground-based Micro Pulse Lidar (MPL) at Skukuza, South Africa. At most altitudes $E_a(\lambda)$ from AATS-14, CPL and MPL agree within 0.02 km^{-1} (at 0.532 μm) or 0.01 km^{-1} (1.06 μm). In the lowest 1 km of the profiles there is tendency for the CPL retrieved $E_a(\lambda)$ to be larger than those from AATS-14. Also, it is important to restate that the lidar extinction retrieval for the cases shown here relies on (and thus is forced to be consistent with) the AERONET (or AATS-14) measurement of total column $\tau_a(\lambda)$.

Finally, we have shown comparisons between aerosol optical depths measured by the AATS-14 and AERONET retrieved over land and over water, and four spaceborne sensors

(TOMS, MODIS, MISR and ATSR-2). For TOMS, two out of three of these comparisons were within the error bars of the measurements. A comparison between AATS-14 and MODIS over water led to excellent agreement, but in a case study over land in Zambia the MODIS algorithm significantly underestimated the aerosol optical depth. Three detailed comparisons of the measurements from the airborne AATS-14 and MISR led to the conclusion that to reproduce the spectral slope of the aerosol optical depth, as measured by AATS-14 and AERONET, the MISR algorithm needs a finer size grid of spherical, non-absorbing aerosols, and it also needs to include smaller particles. One comparison between the AATS-14 and ATSR-2 over water showed agreement (within the error bars) at all wavelengths. The MODIS and ATSR-2 cases shown here represent the first published comparison of aerosol optical depths at 1.2 and 1.6 μm wavelengths.

Acknowledgements

Thanks are due to the dedicated efforts of the University of Washington's Convair-580 team, without whom the measurements described here would not have been obtained. We also express our thanks to the Pietersburg airport personnel, and to the local SAFARI 2000 organizers. We also would like to thank the Ozone Processing Team at NASA Goddard Space Flight Center for making available TOMS EP data.

This research was conducted as part of the Southern African Regional Science Initiative (SAFARI 2000). Funding to NASA Ames was provided by NASA's Earth Observing System Inter-Disciplinary Science (EOS-IDS) Program, Radiation Sciences Program, and Total Ozone Mapping Spectrometer (TOMS) Program (Program Codes 291-01-91-45, 622-44-75-10, and 621-14-01-00, respectively). Funding to the University of Washington was provided by NASA (grants NAG5-9033, NAG5-7075) and NSF's Division of Atmospheric Science (grant ATM-9901624). Work of CRG and GdL is supported by the Netherlands Space Research Foundation

(SRON), under contract EO-037. The ATSR-2 data were provided by the European Space Agency (ESA-ESRIN), contract AO03.280.

References

Abdou W. A., M. C. Helmlinger, D. J. Diner, J. E. Conel, S. H. Pilorz, J. V. Martonchik, C. Gatebe, M. King, and T. Arnold, Sua Pan surface bidirectional reflectance: A validation experiment of the Multi-angle Imaging SpectroRadiometer (MISR) at SAFARI 2000. *J. Geophys. Res.*, this issue.

Annegarn H., R. Swap, S. Piketh, P. Hobbs, A. Queface, T. Freiman, D. Diner, and J. Kanyanga, "The river of smoke": Characteristics of the southern African springtime biomass burning haze. *J. Geophys. Res.*, this issue.

Campbell J., E. J. Welton, J. D. Spinhirne, S.-C. Tsay, Q. Ji, M. Barenbrug, S. J. Piketh, C. J. Bollig, and B. N. Holben, Micropulse lidar observations of smoke and haze over northeastern South Africa: Comparisons between the SAFARI 2000 and ARREX-1999 Dry Season campaigns. *J. Geophys. Res.*, this issue.

Chu, D. A., Y. J. Kaufman, C. Ichoku, L. A. Remer, D. Tanré, and B. N Holben, Validation of MODIS aerosol optical depth retrieval over land. *Geophys. Res. Lett*., in press, 2002.

Clough S. A., and M. J. Iacono, "Line-by-line calculations of atmospheric fluxes and cooling rates II: Application to carbon dioxide, ozone, methane, nitrous oxide, and the halocarbons," *J. Geophys. Res., 100*, 16,519-16,535, 1995.

Diner, D. J., W. A. Abdou, J. E. Conel, K. A. Crean, B. J. Gaitley, M. Helmlinger, R. A. Kahn, J. V. Martonchik, S. H. Pilorz, and B. N. Holben, MISR aerosol retrievals over southern Africa during the SAFARI 2000 dry season campaign, *Geophys. Res. Lett*., *28*, 3127-3130, 2001.

Diner, D. J., L. M. Barge, C. J. Bruegge, T. G. Chrien, J. E. Conel, M. L. Eastwood, J. D. Garcia, M. A. Hernandez, C. G. Kurzweil, W. C. Ledeboer, N. D. Pignatano, C. M. Sarture, and B.

G. Smith, The Airborne Multi-angle Imaging SpectroRadiometer (AirMISR): Instrument description and first results, *IEEE Transact. Geosci. Rmt. Sensing*, *36*, 1339-1349, 1998.

Dubovik, O., B. Holben, T. F. Eck, A. Smirnov, Y. J. Kaufman, M. D. King, D. Tanré, and I. Slutsker, Variability of absorption and optical properties of key aerosol types observed in worldwide locations, *J. Atmos. Sci.*, *59*, 590-608, 2002.

Eck T. F., B. N. Holben, D. E. Ward, M. M. Mukelabai, O. Dubovik, A. Smirnov, J. S. Schafer, N. C. Hsu, S. J. Piketh, A. Queface, J. Le Roux, R. J. Swap, and I. Slutsker, Variability of biomass burning aerosol optical characteristics in southern Africa during the SAFARI 2000 dry season campaign and a comparison of single scattering albedo estimates from radiometric measurements. *J. Geophys. Res.*, this issue

Eck, T. F., B. N. Holben, D. E. Ward, O. Dubovik, J. S. Reid, A. Smirnov, M. M. Mukelabai, N. C. Hsu, N. T. O'Neill, and I. Slutsker, Characterization of biomass burning aerosols in Zambia during the 1997 ZIBBEE field campaign, *J. Geophys. Res*., *106*, 3425-3448, 2001.

Eck T. F., Holben B. N, Reid J. S., Dubovik O., Smirnov A., O'Neill N. T. O., Slutsker I., and Kinne S., Wavelength dependence of the optical depth of biomass burning, urban, and desert dust aerosols, *J. Geophys. Res*., *104*, 31,333-31,349, 1999.

Gonzàlez Jorge, H. and Ogren, J. A., Sensitivity of retrieved aerosol properties to assumptions in the inversion of spectral optical depths. *J. Atmos. Sci*., *53*, 3669-3683. 1996.

Greenblatt G. D., J. J. Orlando, J. B. Burkholder, and A. R. Ravishankara, Absorption measurements of oxygen between 330 and 1140 nm, *J. Geophys. Res*., *95*, 18,577-15,582, 1990.

Hao, W. M., D. E. Ward, R. A. Susott, R. E. Babbitt, B. L. Nordgren, B. N. Holben, T. Eck. Y. J. Kaufman, Aerosol Optical Depths in Southern Africa during the Dry Season in 2000, *Int. J. of Remote Sensing*, to submitted March 31, 2002.

Harder J. W., J. W. Brault, P. V. Johnston, and G. H. Mount, Temperature dependent NO_2 cross sections at high spectral resolution, *J. Geophys. Res.*, *102*, 3861-3879, 1997.

Hobbs, P.V., Technical Appendix: An overview of the University of Washington's airborne measurements in the SAFARI 2000 field study in southern Africa, *J. Geophys. Res*., D???, yyy-zzz, 2003a.

Hobbs, P.V., Clean air slots amid dense atmospheric pollution in southern Africa, *J. Geophys. Res.*, this issue, b.

Hobbs, P.V., Summary of flights and types of data collected aboard the University of Washington's Convair-580 research aircraft in the SAFARI 2000 field study in Sothern Africa from 10 August through 18 September 2000. *Cloud and Aerosol Research Group*, Atmospheric Sciences, University of Washington, 2001

Hobbs, P.V., Clean air slots amid atmospheric pollution, *Nature*, *415*, 861, 2002.

Holben, B. N., T. Eck, I. Slutsker, D. Tanré, J. B. Buis, A. Setzer, E. Vermote, J. A. Reagan, Y. A. Kaufman, T. Nakajima, F. Lavenu, I. Jankowiak, and A.Smirnov, AERONET – A Federated Instrument Network and Data Archive for Aerosol Characterization. *Rem. Sens. Env.*, *66*, 1-16, 1998.

Holben, B. N., D. Tanré, A. Smirnov, T. F. Eck, I. Slutsker, N. Abuhassan, W. W. Newcomb, J. Schafer, B. Chatenet, F. Lavenue, Y. J. Kaufman, J. Vande Castle, A. Setzer, B. Markham, D. Clark, R. Frouin, R. Halthore, A. Karnieli, N. T. O'Neill, C. Pietras, R. T. Pinker, K.

Voss, and G. Zibordi, An emerging ground-based aerosol climatology, Aerosol Optical Depth from AERONET, *J. Geophys. Res*., *106*, 12 067-12 097, 2001.

Ichoku, C., D. A. Chu, S. Mattoo, Y. J. Kaufman, L.A. Remer, D. Tanré, I. Slutsker, and B. N. Holben, A Spatio-Temporal Approach for Global Validation and Analysis of MODIS Aerosol Products. *Geophys. Res. Lett*., in press, 2002.

Kahn, R., P. Banerjee, and D. McDonald, The sensitivity of multiangle imaging to natural mixtures of aerosols over ocean, *J. Geophys. Res*., *106*, 18,219-18,238, 2001.

Kaufman, Y. J., D. Tanré, L. A. Remer, E. F. Vermote, A. Chu, and B. N. Holben, Operational remote sensing of tropospheric aerosol over land from EOS moderate resolution imaging spectroradiometer, *J. Geophys. Res*., *102*, 17,051-17,067, 1997.

King, M. D., Sensitivity of constrained linear inversions to the selection of the Lagrange multiplier. *J. Atmos. Sci*., *39*, 1356-1369, 1982.

King, M. D., Byrne, D. M., Herman, B. M. and Reagan, J. A., Aerosol size distributions obtained by inversion of spectral optical depth measurements. *J. Atmos. Sci*., *35*, 2153-2167, 1978.

Magi, B. I., P. V. Hobbs, and B. Schmid, Vertical profiles of light scattering, light absorption and single scattering albedo during the dry, biomass burning season in southern Africa and comparisons of in situ and remote sensing measurements of aerosol optical depths, *J. Geophys. Res.*, this issue.

Martonchik, J. V., D. J. Diner, R. Kahn, T. P. Ackerman, M. M. Verstraete, B. Pinty, and H. R. Gordon, Techniques for the retrieval of aerosol properties over land and ocean using multi-angle imaging. *IEEE Trans. Geosci. Rem. Sens*., *36*, 1212-1227, 1998.

McGill M., D. Hlavka, W. Hart, J. Spinhirne, S. Scott, and B. Schmid. The cloud physics lidar: instrument description and initial measurement results. *Appl. Opt*., in press, 2002.

McGill M., D. L. Hlavka, W. D. Hart, J. D. Spinhirne, Airborne lidar measurements of optical properties of boundary layer aerosol during the SAFARI 2000 field campaign, *J. Geophys. Res*., this issue.

Michalsky J., M. Beauharnois, J. Berndt, L. Harrsison, P. Kiedron, and Q. Min, O_2-O_2 absorption band identification based on optical depth spectra of the visible and near-infrared, *Geophys. Res. Lett.*, *26*, 1581-1584, 1999.

Remer L. A., D. Tanré, Y. J. Kaufman, C. Ichoku, S. Mattoo, R. Levy, D. A. Chu, B. N Holben O. Dubovik, A. Smirnov, J. V. Martins, R.-R. Li, and Z. Ahmad, Validation of MODIS aerosol retrieval over ocean. *Geophys. Res. Lett*., in press, 2002.

Robles-Gonzalez, C., J. P. Veefkind and G. de Leeuw, Mean aerosol optical depth over Europe in August 1997 derived from ATSR-2 data. *Geophys. Res. Lett*. *27*, 955-959, 2000.

Robles-Gonzalez, C., G. de Leeuw, P. J. H. Builtjes, M. van Loon and M. Schaap, Spatial variation of aerosol properties derived from satellite observations, in preparation.

Russell, P. B., J. M. Livingston, E. G. Dutton, R. F. Pueschel, J. A. Reagan, T. E. Defoor, M. A. Box, D. Allen, P. Pilewskie, B. M. Herman, S. A. Kinne, and D. J. Hofmann, Pinatubo and pre-Pinatubo optical-depth spectra: Mauna Loa measurements, comparisons, inferred particle size distributions, radiative effects, and relationship to lidar data. *J. Geophys. Res*., *98*, 22'969-22'985, 1993.

Russell, P. B., P. V. Hobbs, and L. L. Stowe, Aerosol properties and radiative effects in the United States Mid-Atlantic haze plume: An overview of the Tropospheric Aerosol Radiative Forcing Observational Experiment (TARFOX), *J. Geophys. Res*., *104*, 2213-2222, 1999a.

Russell, P. B., J. M. Livingston, P. Hignett, S. Kinne, J. Wong, and P. V. Hobbs, Aerosol-induced radiative flux changes off the United States Mid-Atlantic coast, Comparison of

values calculated from sunphotometer and in situ data with those measured by airborne pyranometer, *J. Geophys. Res., 104*, 2289-2307, 1999b.

Schermaul, R., R.C.M. Learner, D.A. Newnham, R.G. Williams, J. Ballard, N.F. Zobov, D. Belmiloud, and J. Tennyson, The water vapor spectrum in the region 8600 - 15000 cm^{-1}: experimental and theoretical studies for a new spectral line database. II: Linelist construction, *J. Mol. Spectrosc*., *208*, 43-50, 2001.

Schmid, B., and C. Wehrli, Comparison of sun photometer calibration by Langley technique and standard lamp, *Appl. Opt*., *34*, 4500-4512, 1995.

Schmid, B., K. J. Thome, P. Demoulin, R. Peter, C. Mätzler, and J. Sekler, Comparison of modeled and empirical approaches for retrieving columnar water vapor from solar transmittance measurements in the 0.94 micron region, *J. Geophys. Res., 101*, 9345-9358, 1996.

Schmid, B., C. Mätzler, A. Heimo, and N. Kämpfer, Retrieval of optical depth and size distribution of tropospheric and stratospheric aerosols by means of sun photometry. *IEEE Trans. Geosci. Remote. Sens*., *35*, 172-182, 1997.

Schmid, B., P. R. Spyak, S. F. Biggar, C. Wehrli, J. Sekler, T. Ingold, C. Mätzler, and N. Kämpfer, Evaluation of the applicability of solar and lamp radiometric calibrations of a precision Sun photometer operating between 300 and 1025 nm, *Appl. Opt., 37*, 3923-3941, 1998.

Schmid B., J. Michalsky, R. Halthore, M. Beauharnois, L. Harrison, J. Livingston, P. Russell, B. Holben, T. Eck, and A. Smirnov, Comparison of Aerosol Optical Depth from Four Solar Radiometers During the Fall 1997 ARM Intensive Observation Period, *Geophys. Res. Lett*., *26*, 2725-2728, 1999.

Schmid, B., J. M. Livingston, P. B. Russell, P. A. Durkee, H. H. Jonsson, D. R. Collins, R. C. Flagan, J. H. Seinfeld, S. Gassó, D. A. Hegg, E. Öström, K. J. Noone, E. J. Welton, K. J. Voss, H. R. Gordon, P. Formenti, and M. O. Andreae, Clear sky closure studies of lower tropospheric aerosol and water vapor during ACE 2 using airborne sunphotometer, airborne in-situ, space-borne, and ground-based measurements, *Tellus*, *B 52*, 568-593, 2000.

Schmid B., J. J. Michalsky, D. W. Slater, J. C. Barnard, R. N. Halthore, J. C. Liljegren, B. N. Holben, T. F. Eck, J. M. Livingston, P. B. Russell, T. Ingold, and I. Slutsker, Comparison of columnar water-vapor measurements from solar transmittance methods. *Appl. Opt., 40*, 1886-1896, 2001.

Schneider W., G. K. Moortgat, G. S. Tyndall and J. P. Burrows, Absorption cross-sections of NO_2 in the uv and visible region (200-700 nm) at 298 K, *J. Photochem. Photobiol., A: Chem*., *40*, 195-217, 1987.

Spinhirne, J. D., J. A. R. Rall, and V. S. Scott, Compact Eye Safe Lidar Systems, *Rev. Laser Eng.*, *23*, 112-118, 1995.

Swap, R. J. et al, SAFARI 2000 overview paper. *J. Geophys. Res.*, this issue.

Tanré, D., Kaufman, Y. J., Herman, M., and S. Mattoo, Remote sensing of aerosol properties over oceans using MODIS/EOS spectra radiances, *J. Geophys. Res.*, *102*, 16,971-16,988, 1997.

Torres, O., P. K. Bhartia, J. R. Herman, Z. Ahmad and J. Gleason: Derivation of aerosol properties from satellite measurements of backscattered ultraviolet radiation: Theoretical basis. *J. Geophys. Res.*, *103*, 17,099-17,110, 1998.

Torres, O., P. K. Bhartia, J. R. Herman, A. Sinyuk, P. Ginoux and B. Holben, A long-term record of aerosol optical depth from TOMS observations and comparison to AERONET measurements, *J. Atmos. Sci*., *59*, 398-413, 2002.

Veefkind, J. P., G. de Leeuw, and P.A. Durkee, Retrieval of aerosol optical depth over land using two-angle view satellite radiometry during TARFOX, *Geophys. Res. Lett.*, *25*, 3135-3138, 1998.

Veefkind J. P., G. de Leeuw, P. A. Durkee, P. B. Russell, P. V. Hobbs, and J. M. Livingston, Aerosol optical depth retrieval using ATSR-2 and AVHRR data during TARFOX, *J. Geophys. Res.*, *104*, 2253-2260, 1999.

Welton, E. J., J. R. Campbell, T. A. Berkoff, J. D. Spinhirne, S. Tsay, B. Holben, and M. Shiobara, The Micro-pulse Lidar Network (MPL-Net), *Int. Laser Rad. Conf. Proc*., in press, 2002.

Zhao, T. X.-P., L. L. Stowe, A. Smirnov, A., D. Crosby, J. Sapper, and C. R. McClain, Development of a global validation package for satellite oceanic aerosol optical thickness retrieval based on AERONET observations and its application to NOAA/NESDIS operational aerosol retrievals, *J. Atmos. Sci., 59*, 294-312, 2002.

Table 1. University of Washington's Convair-580 low-altitude fly-by's at AERONET sites in SAFARI-2000.

Site	Country	Latitude (S)	Longitude (E)	Altitude (m)	Aircraft Altitude (m)	Separation (km)	Date (year 2000) Time (UTC, hr:min)	Subplot in Figure 3
Skukuza	South Africa	24°59'	31°35'	150	384	31	Aug 17. 08:06	a)
					429	45	Aug 17. 09:37	b)
					324	3	Aug 22.10:07	c)
Inhaca Island	Mozambique	26°02'	32°54'	73	61	4	Aug 24, 08:37	d)
Kaoma	Zambia	14°47'	24°47'	1179	1261	34	Sep 1, 09:09	e)
Sua Pan	Botswana	20°31'	26°04'	900	947	12	Sep 3, 08:50	f)
Senanga	Zambia	16°06'	23°17'	1025	1172	9	Sep 6, 07:56	g)
Mongu	Zambia	15°15'	23°09'	1107	1041	11	Sep 6, 08:15	h)
					1228	2	Sep 6, 09:14	i)
Etosha Pan	Namibia	19°10'	15°54'	1131	1142	20	Sep 16, 09:24	k)
					1195	7	Sep 16, 10:53	l)

Figures

Figure 1: Map of study area, showing many of the locations over which measurements were obtained from the University of Washington's Convair-580 research aircraft in SAFARI 2000 [from *Hobbs*, 2001].

Figure 2: Scatter plot comparison of $\tau_a(\lambda)$ from AERONET and AATS-14 during low altitude fly-by's at each of the seven AERONET wavelengths. The identity line is indicated by the broken line, the full line is the least-squares fit to the data.

Figure 3: Comparison of $\tau_a(\lambda)$ spectra from AERONET and AATS-14 during low altitude fly-by's. Information pertaining to each of the subplots a) through l) is given in Table 1. The lines are fits of eq. 1 to the AATS-14 data.

Figure 4: Time traces of $\tau_a(\lambda)$ and spectral parameters obtained from four consecutive penetrations by the Convair-580 of a smoke plume originating from a flaming hot grass-fire on August 17, 2000 in the Kruger National Park North of Skukuza (24°28'S/31°50'E). Data gaps are explained in the text. Time axis is UTC in decimal hours.

Figure 5: Map of $\tau_a(0.499\ \mu m)$ of a smoke plume originating from a flaming hot grass-fire on August 17, 2000, in the Kruger National Park North of Skukuza (24°28'S/31°50'E). The $\tau_a(\lambda)$ measurements are taken at each individual white dot along the white Convair-580 flight track. A triangle-based linear interpolation is used to fill in τ_a values between the flight tracks. Size of the map is $22.25 \times 22.25\ km^2$.

Figure 6: a) $\tau_a(\lambda)$ spectra measured in and outside of a smoke plume originating from a flaming hot grass-fire on August 17, 2000, in the Kruger National Park North of Skukuza (24°28'S/31°50'E). Also shown is the $\tau_a(\lambda)$ difference spectrum. b) Area size distributions inverted from the $\tau_a(\lambda)$ spectra in a). Three inversion results are shown per case obtained by using three different initial estimates of the size distribution. Solid lines in a) are $\tau_a(\lambda)$ spectra computed from the size distributions in b).

Figure 7: Vertical profiles of $\tau_a(\lambda)$, aerosol extinction, columnar water vapor, and water vapor density, for nine different locations and dates. All locations can be found on the map in Figure 1. The shaded areas depict the altitude above sea level of the underlying terrain. The wavelengths are indicated in units of μm.

Figure 8: Comparison of aerosol vertical profiles from AATS-14 on the Convair-580 aircraft, CPL on the ER-2 aircraft, and ground-based MPL over Skukuza, South Africa, August 22, 2000. The shaded area depicts the altitude above sea level of the underlying terrain.

Figure 9: Comparison of aerosol vertical profiles from AATS-14 on the Convair-580 aircraft, CPL on the ER-2 aircraft over Inhaca Island, Mozambique, August 24, 2000.

Figure 10: Same as Figure 9 but for Senanga, Zambia, September 6, 2000. The shaded area depicts the altitude above sea level of the underlying terrain.

Figure 11: Same as Figure 9 but for Mongu, Zambia, September 6, 2000. The shaded area depicts the altitude above sea level of the underlying terrain.

Figure 12: Same as Figure 9 but off Namibian Coast, September 11, 2000.

Figure 13: Comparison of TOMS retrieved τ_a at 0.38 μm with AATS-14 during low altitude passes of the Convair-580 within or near a TOMS pixel.

Figure 14: Comparison of MODIS retrieved $\tau_a(\lambda)$ over water (top) and over land (bottom) with AERONET Sun/sky radiometers and with AATS-14 during low altitude passes of the Convair-580 within or near a MODIS pixel. Dashed lines indicate the expected MODIS $\tau_a(\lambda)$ retrieval error.

Figure 15: Comparison of MISR retrieved $\tau_a(\lambda)$ on with the Skukuza AERONET Sun/sky radiometer and with AATS-14 during a low altitude pass of the Convair-580 within one 17.6×17.6 km^2 MISR region on August 22, 2000.

Figure 16: MISR data over northwestern Botswana acquired on September 3, 2000 (Terra Orbit 3786). Left image is a red, green, blue (RGB) composite of radiometrically calibrated, geo-located data from the nadir camera, right image shows best-fit τ_a(0.558 μm); the pixellation shows individual 17.6×17.6 km^2 regions.

Figure 17: Comparison of MISR retrieved $\tau_a(\lambda)$ with the Sua Pan AERONET Sun/sky radiometer and with AATS-14 during a low altitude pass of the Convair-580 within two adjacent 17.6×17.6 km^2 MISR regions on September 3, 2000. The AERONET instrument was located in the 17.6×17.6 km^2 MISR region shown in the top plot, but the data are repeated in the bottom plot for reference purposes.

Figure 18: Comparison of MISR retrieved $\tau_a(\lambda)$ with AATS-14 during a low altitude pass of the Convair-580 within two adjacent 17.6×17.6 km^2 MISR regions off the Namibian Coast on September 11, 2000.

Figure 19: Top: Map of $\tau_a(0.555\ \mu m)$ from ATSR-2 off the Namibian Coast on September 14, 2000. Red line marks coastline. Red filled circle marks approximate position of Convair-580 carrying AATS-14, slightly outside ATSR-2 swath. White patches show areas identified as clouds. Bottom: Comparison of ATSR-2 retrieved $\tau_a(\lambda)$ with AATS-14 during a low altitude pass of the Convair-580 at the position marked in the upper figure. Wide AATS-14 error bars show measurement error, narrow error bars show $\tau_a(\lambda)$ variability (2σ). Green dotted lines indicate predicted uncertainty of ATSR-2 retrieved $\tau_a(\lambda)$.

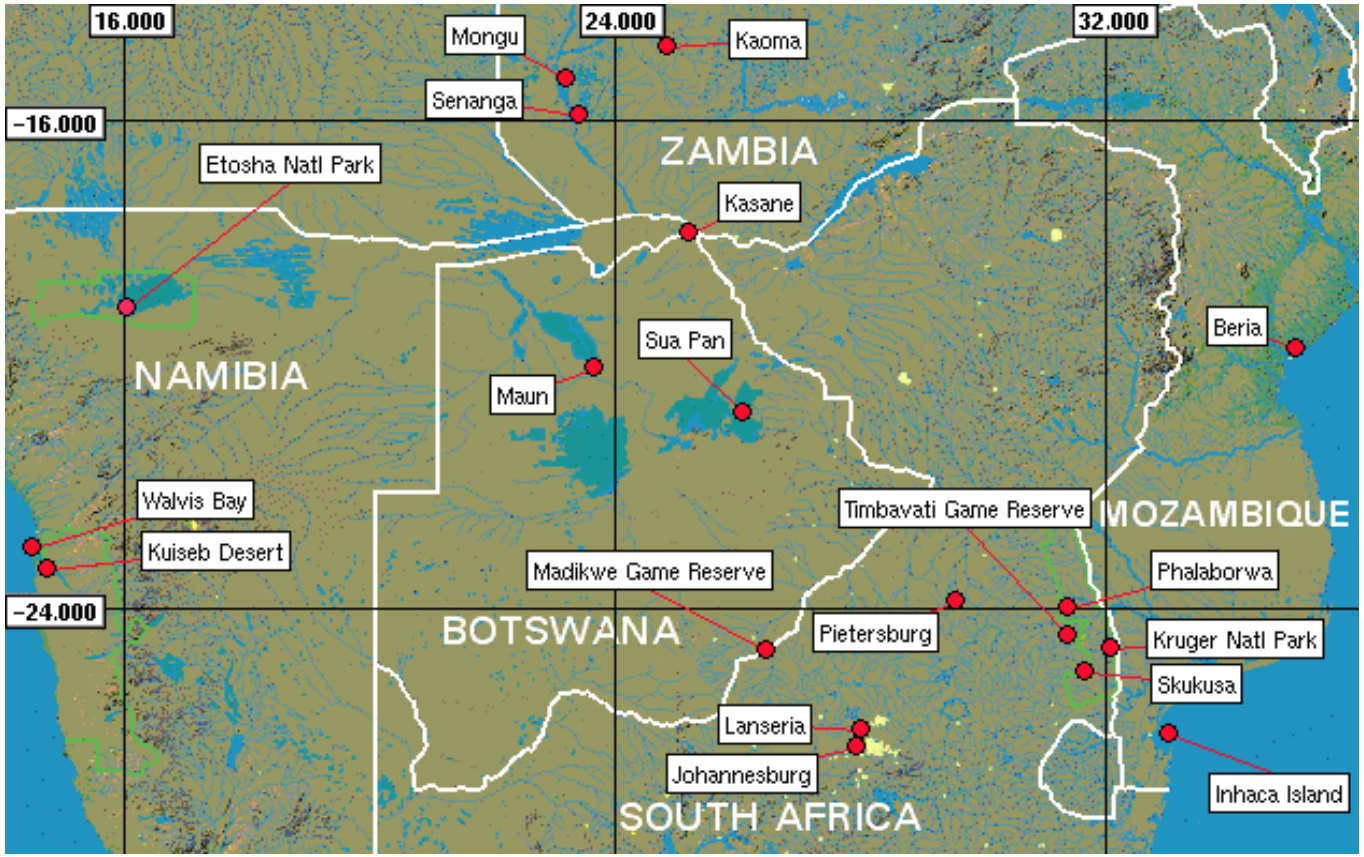
16.000
24.000
32.000
-16.000
-24.000
Mongu
Kaoma
Senanga
ZAMBIA
Etosha Natl Park
Kasane
NAMIBIA
Sua Pan
Beria
Maun
Walvis Bay
Timbavati Game Reserve
MOZAMBIQUE
Kuiseb Desert
Madikwe Game Reserve
Phalaborwa
BOTSWANA
Pietersburg
Kruger Natl Park
Skukusa
Lanseria
Johannesburg
Inhaca Island
SOUTH AFRICA

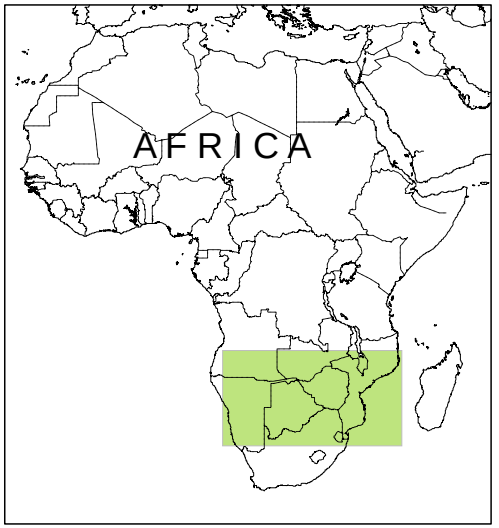
AFRICA

Fig. 1

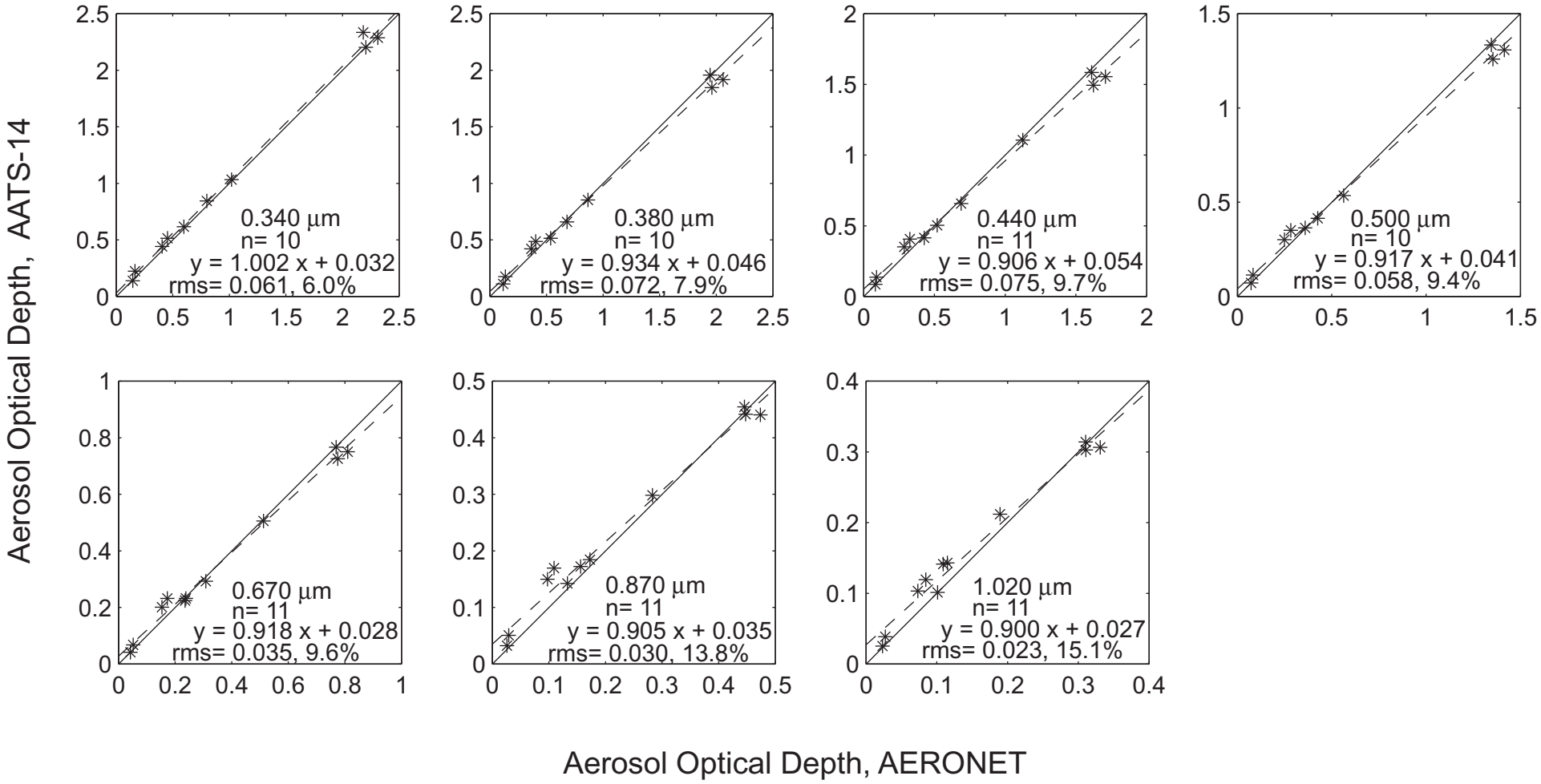
Aerosol Optical Depth, AATS-14
Aerosol Optical Depth, AERONET
0.340 µm
n= 10
y = 1.002 x + 0.032
rms= 0.061, 6.0%
0.380 µm
n= 10
y = 0.934 x + 0.046
rms= 0.072, 7.9%
0.440 µm
n= 11
y = 0.906 x + 0.054
rms= 0.075, 9.7%
0.500 µm
n= 10
y = 0.917 x + 0.041
rms= 0.058, 9.4%
0.670 µm
n= 11
y = 0.918 x + 0.028
rms= 0.035, 9.6%
0.870 µm
n= 11
y = 0.905 x + 0.035
rms= 0.030, 13.8%
1.020 µm
n= 11
y = 0.900 x + 0.027
rms= 0.023, 15.1%

Fig. 2

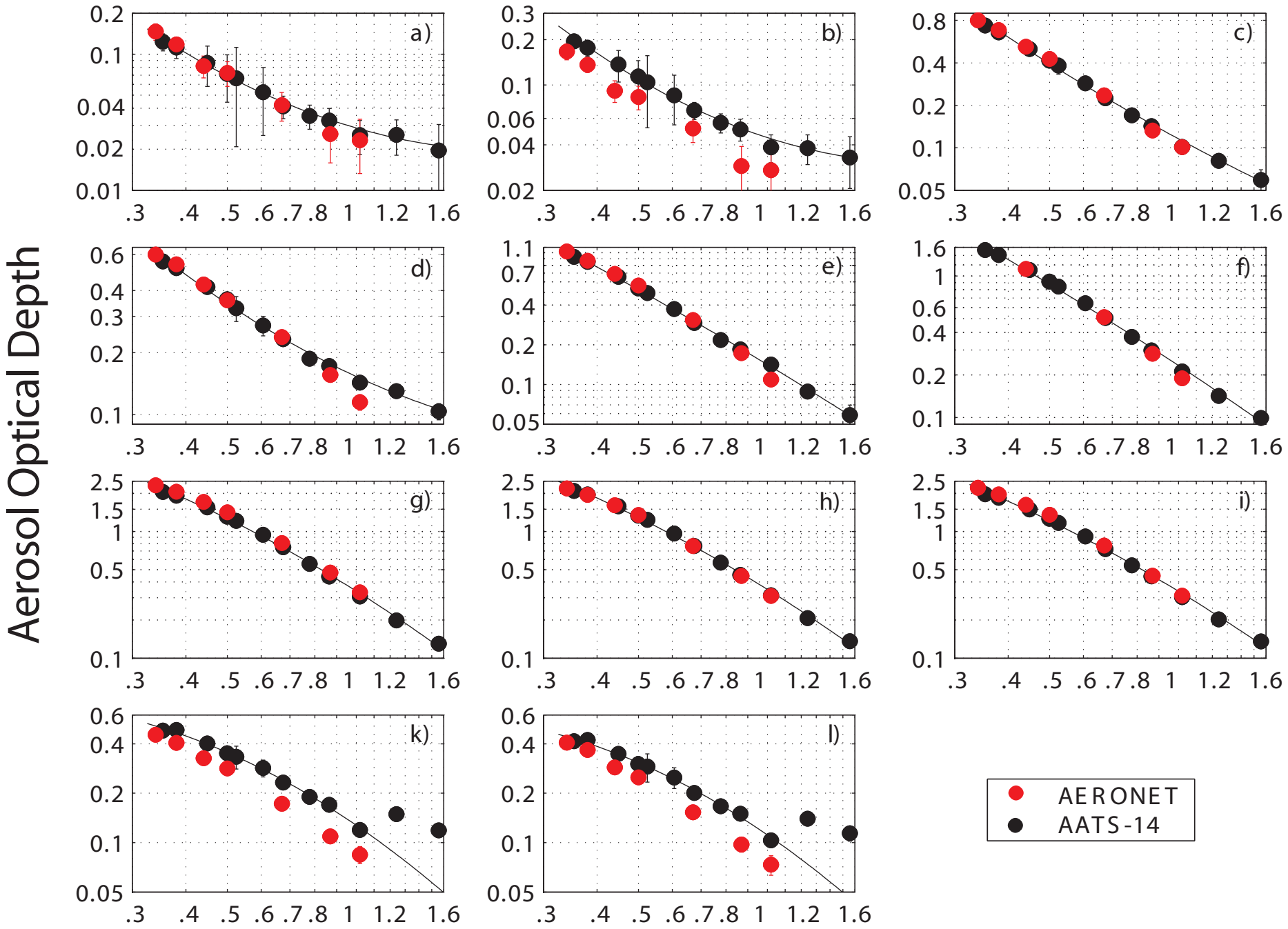
Aerosol Optical Depth
Wavelength (μm)
a)
b)
c)
d)
e)
f)
g)
h)
i)
k)
l)
AERONET
AATS-14

Fig. 3

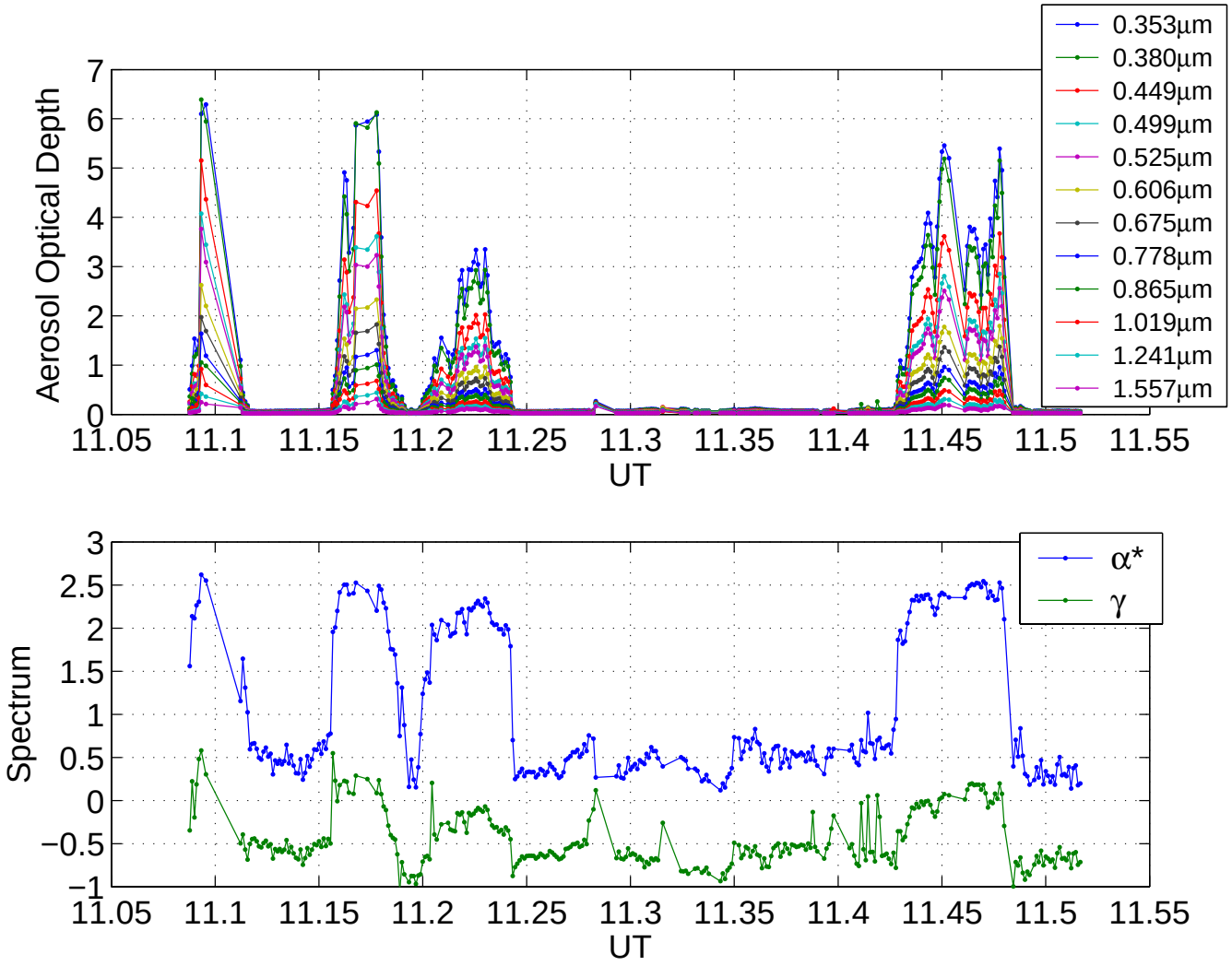
Aerosol Optical Depth
UT
0.353µm
0.380µm
0.449µm
0.499µm
0.525µm
0.606µm
0.675µm
0.778µm
0.865µm
1.019µm
1.241µm
1.557µm
Spectrum
α*
γ

Fig. 4

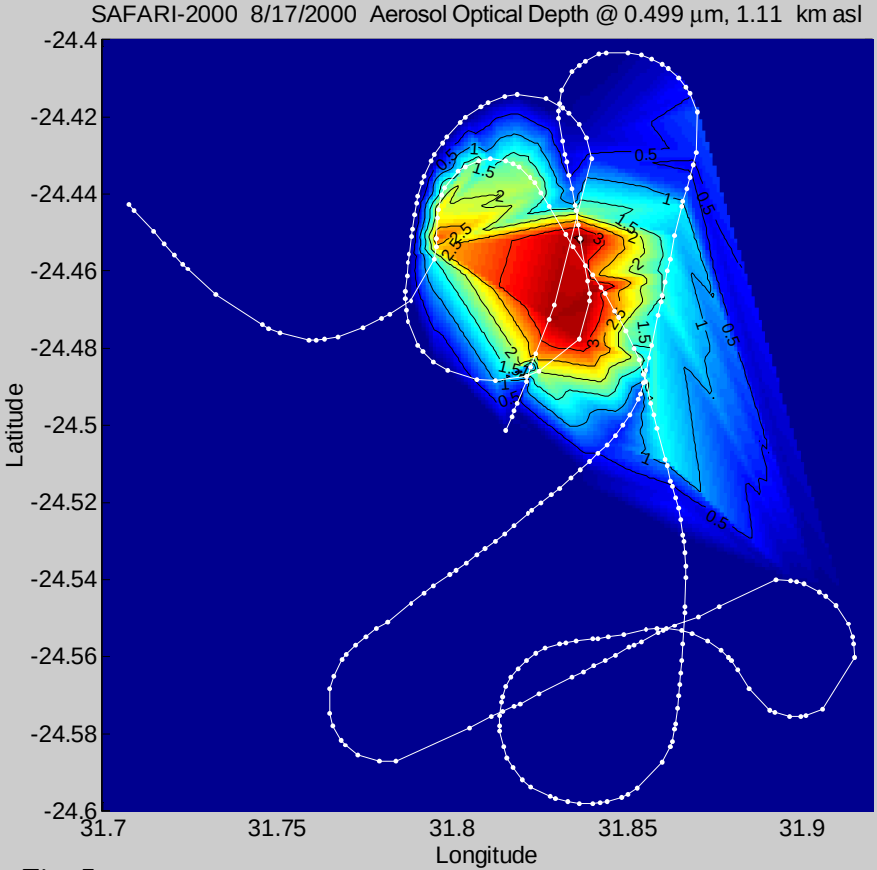
SAFARI-2000 8/17/2000 Aerosol Optical Depth @ 0.499 µm, 1.11 km asl
-24.4
-24.42
-24.44
-24.46
-24.48
-24.5
-24.52
-24.54
-24.56
-24.58
-24.6
Latitude
31.7
31.75
31.8
31.85
31.9
Longitude

Fig. 5

Fig. 6

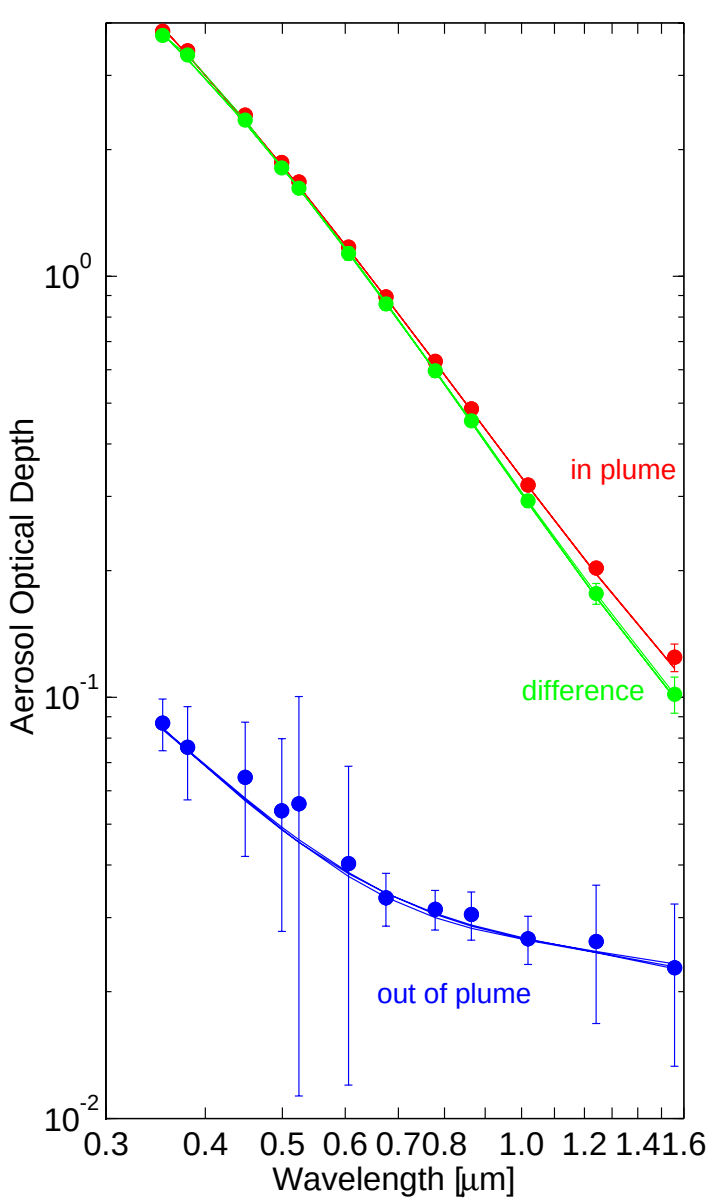
Aerosol Optical Depth
Wavelength [µm]
in plume
difference
out of plume

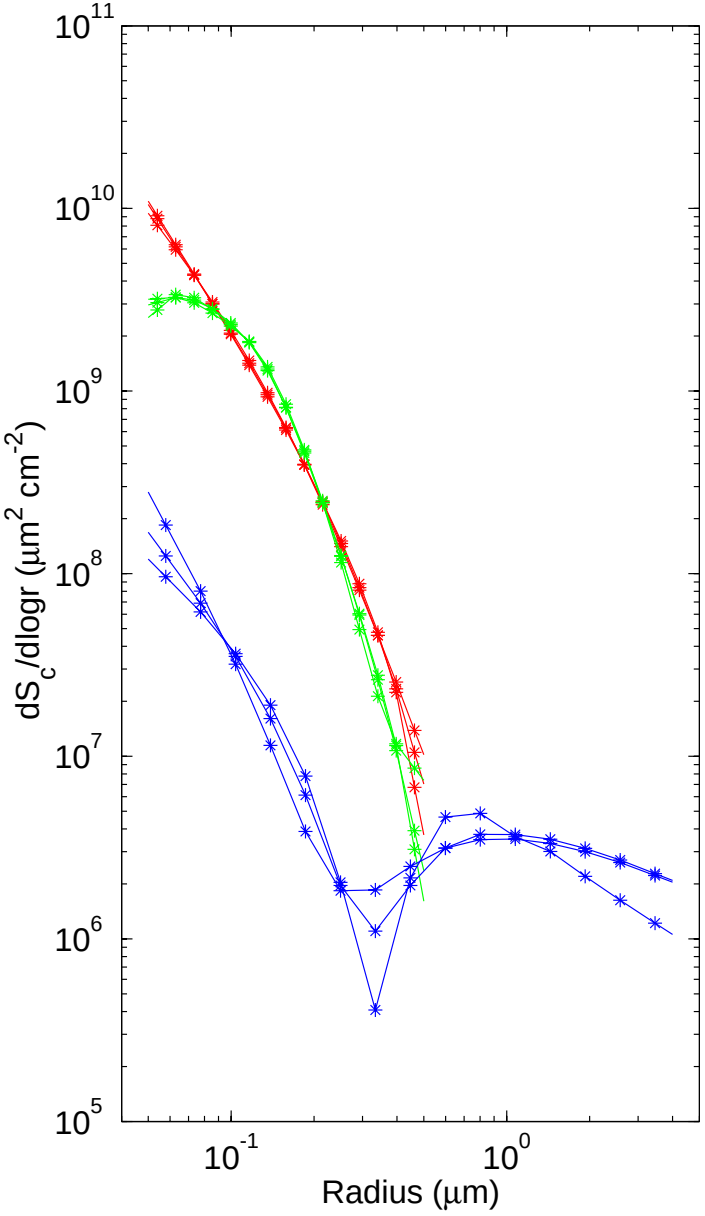
dS$_c$/dlogr (µm^2 cm^{-2})
Radius (µm)

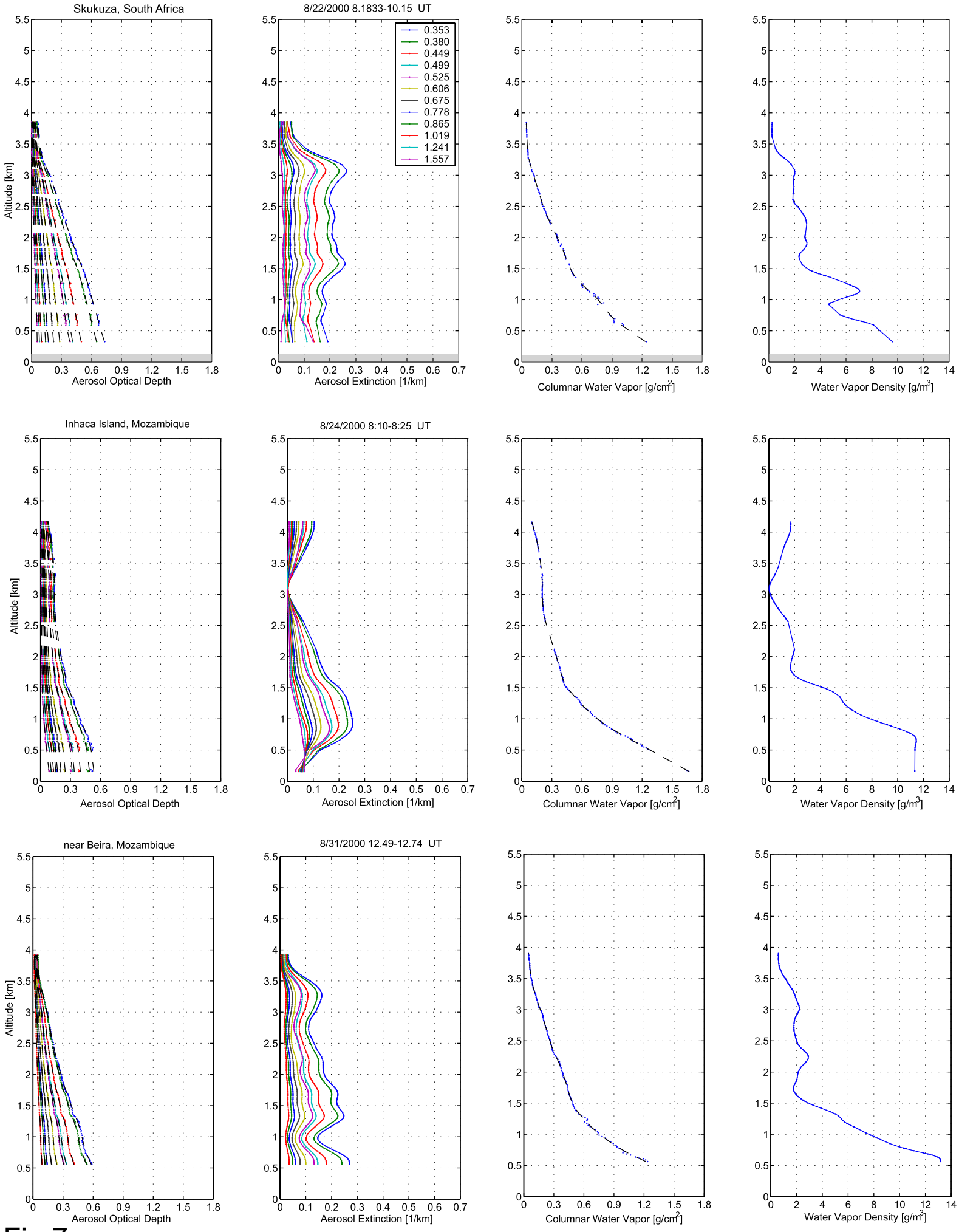
Skukuza, South Africa
8/22/2000 8.1833-10.15 UT
0.353
0.380
0.449
0.499
0.525
0.606
0.675
0.778
0.865
1.019
1.241
1.557
Altitude [km]
Aerosol Optical Depth
Aerosol Extinction [1/km]
Columnar Water Vapor [g/cm2]
Water Vapor Density [g/m3]
Inhaca Island, Mozambique
8/24/2000 8:10-8:25 UT
near Beira, Mozambique
8/31/2000 12.49-12.74 UT

Fig 7

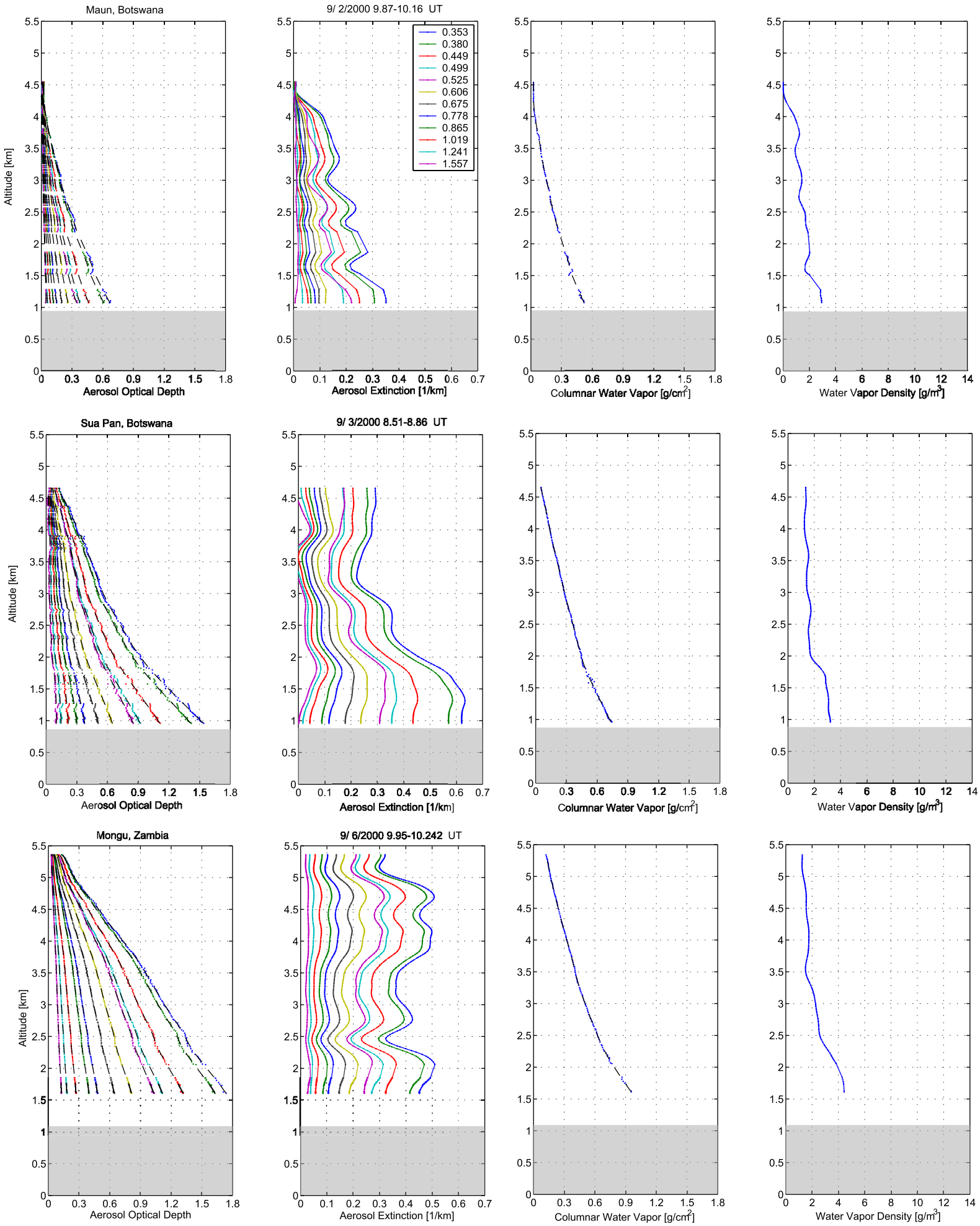

Fig 7 continued

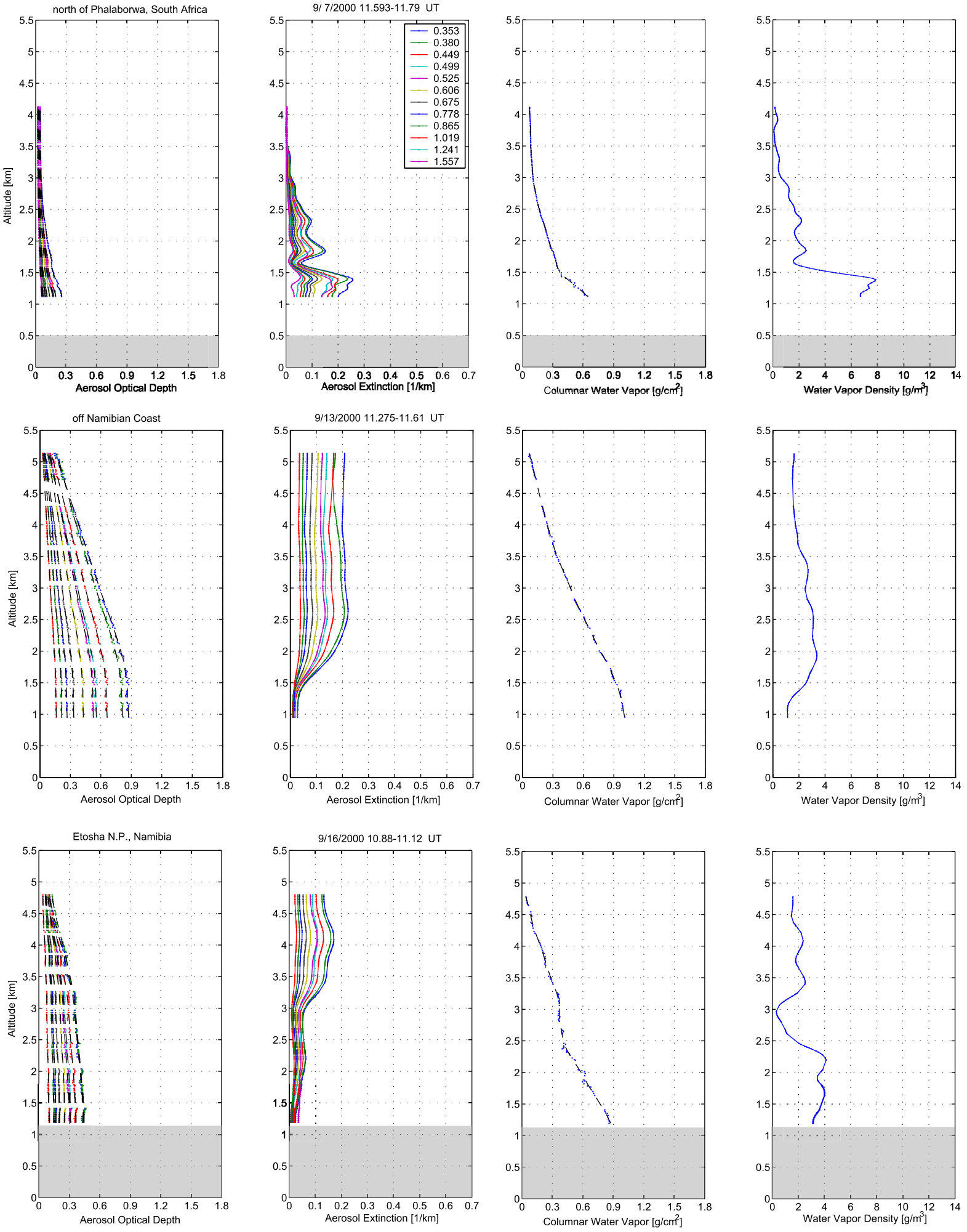

Fig 7 continued

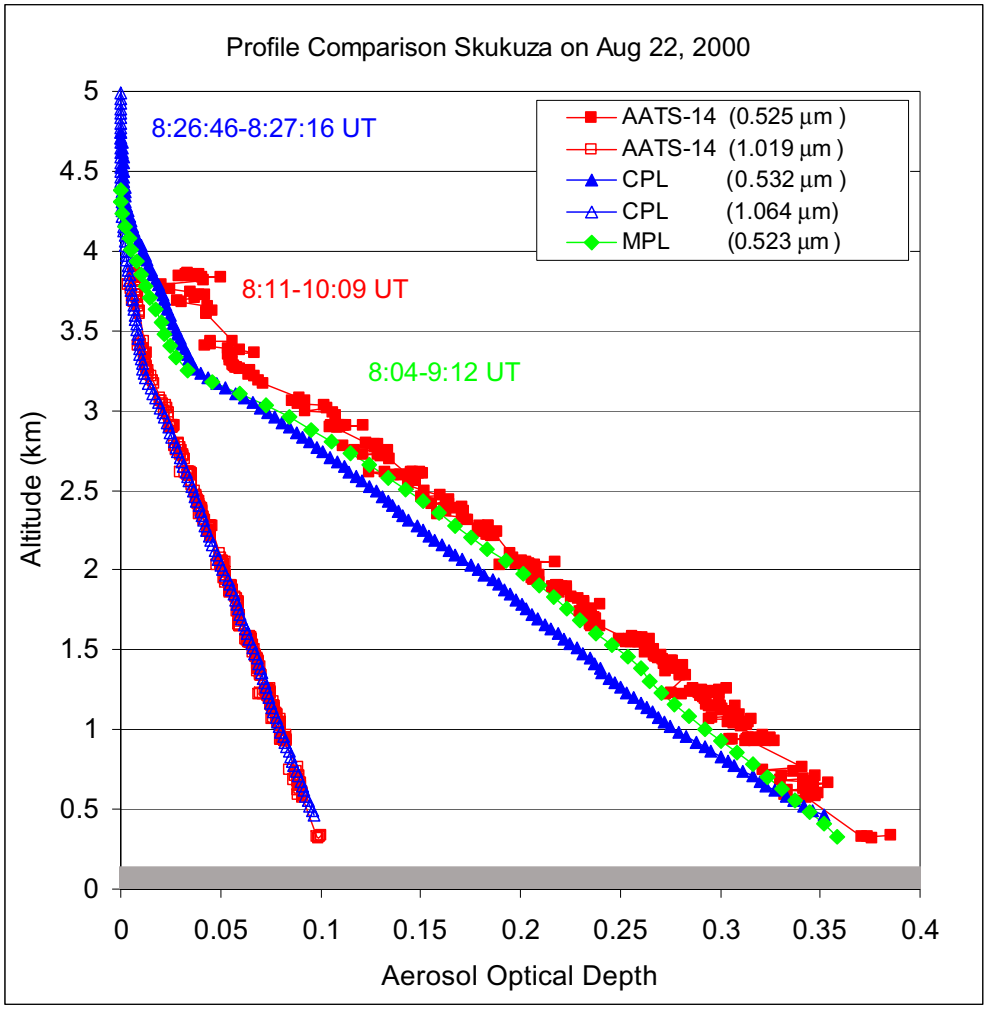
Profile Comparison Skukuza on Aug 22, 2000
8:26:46-8:27:16 UT
8:11-10:09 UT
8:04-9:12 UT
AATS-14 (0.525 µm)
AATS-14 (1.019 µm)
CPL (0.532 µm)
CPL (1.064 µm)
MPL (0.523 µm)
Altitude (km)
Aerosol Optical Depth
0
0.5
1
1.5
2
2.5
3
3.5
4
4.5
5
0.05
0.1
0.15
0.2
0.25
0.3
0.35
0.4

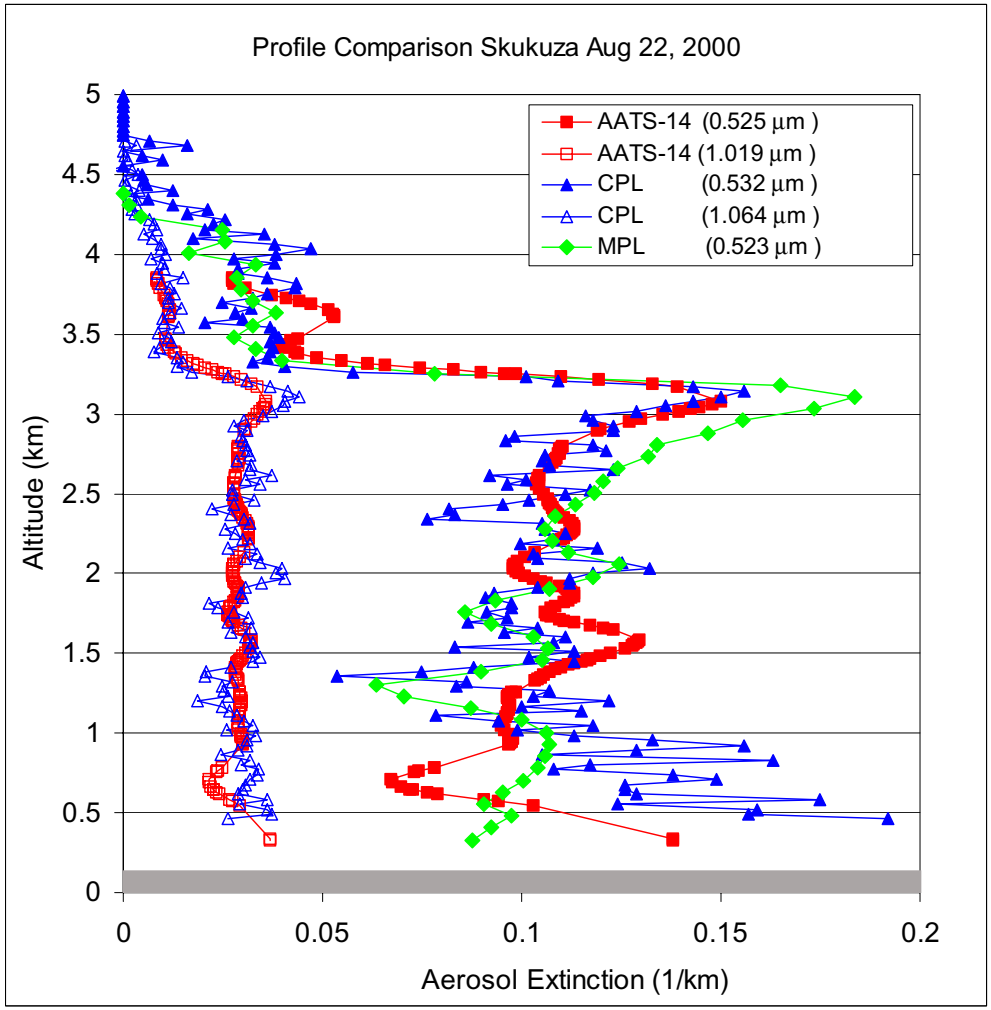
Profile Comparison Skukuza Aug 22, 2000
AATS-14 (0.525 µm)
AATS-14 (1.019 µm)
CPL (0.532 µm)
CPL (1.064 µm)
MPL (0.523 µm)
Altitude (km)
Aerosol Extinction (1/km)
0
0.5
1
1.5
2
2.5
3
3.5
4
4.5
5
0.05
0.1
0.15
0.2

Fig. 8

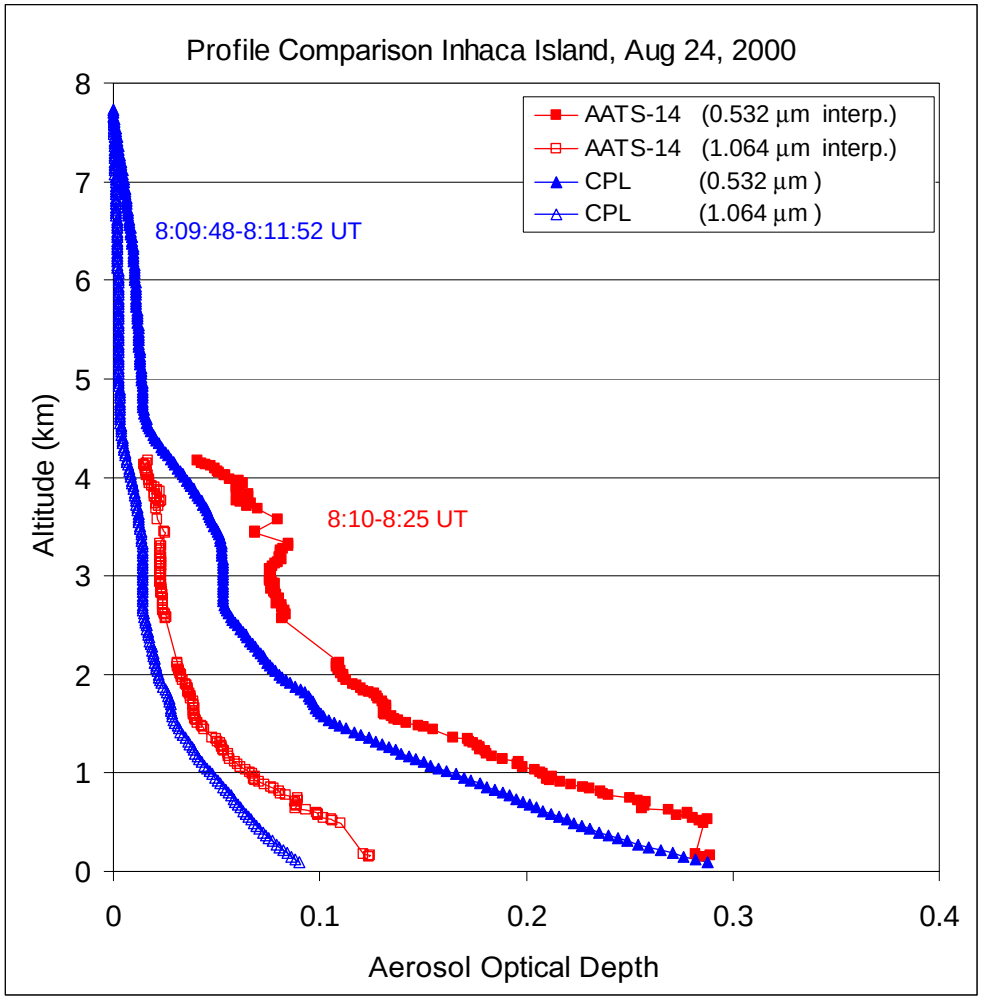
Profile Comparison Inhaca Island, Aug 24, 2000
AATS-14 (0.532 µm interp.)
AATS-14 (1.064 µm interp.)
CPL (0.532 µm)
CPL (1.064 µm)
8:09:48-8:11:52 UT
8:10-8:25 UT
Altitude (km)
Aerosol Optical Depth
0
1
2
3
4
5
6
7
8
0
0.1
0.2
0.3
0.4

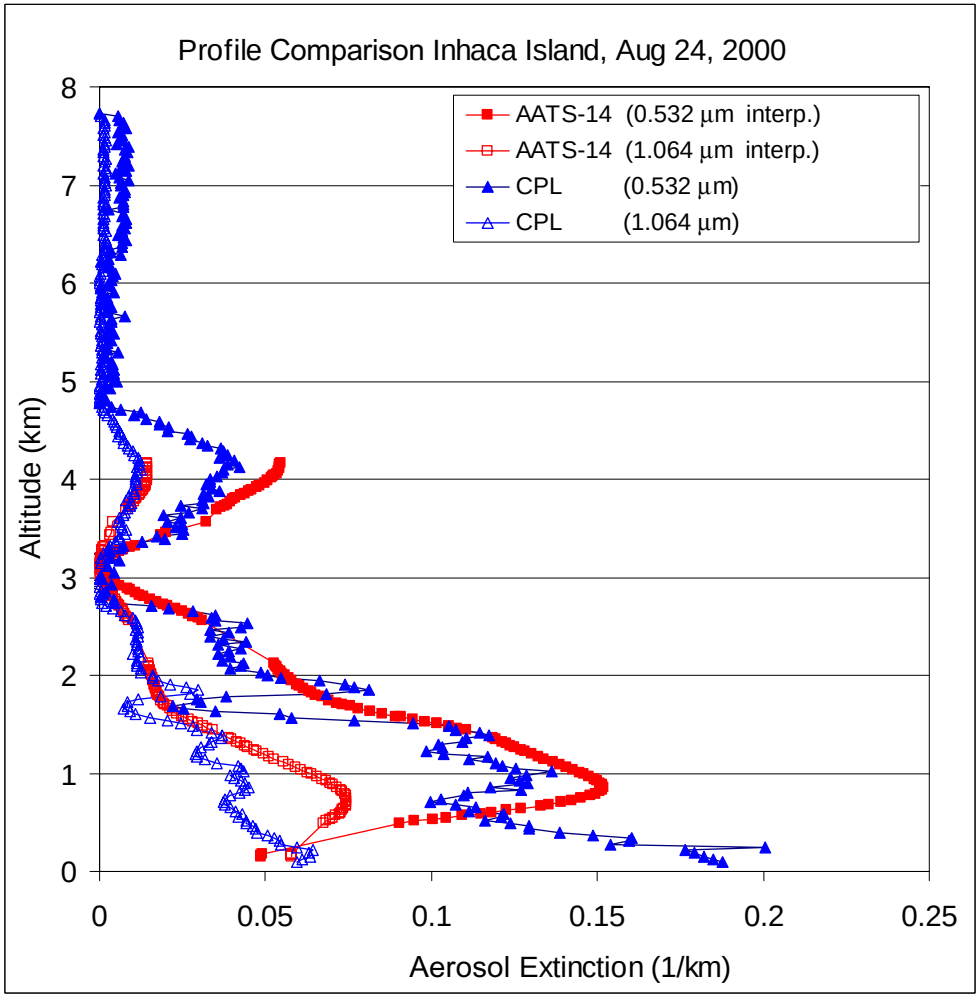
Profile Comparison Inhaca Island, Aug 24, 2000
AATS-14 (0.532 µm interp.)
AATS-14 (1.064 µm interp.)
CPL (0.532 µm)
CPL (1.064 µm)
Altitude (km)
Aerosol Extinction (1/km)
0
1
2
3
4
5
6
7
8
0
0.05
0.1
0.15
0.2
0.25

Fig. 9

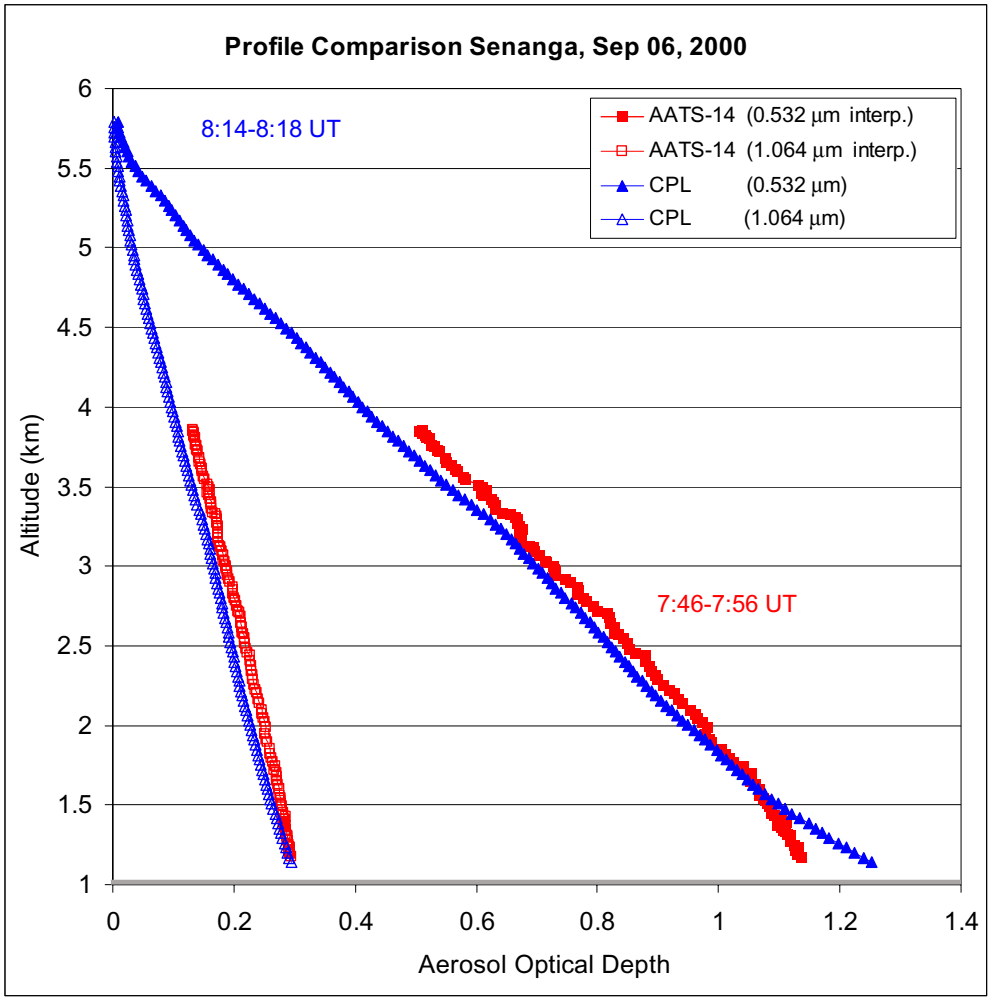
Profile Comparison Senanga, Sep 06, 2000
8:14-8:18 UT
7:46-7:56 UT
AATS-14 (0.532 µm interp.)
AATS-14 (1.064 µm interp.)
CPL (0.532 µm)
CPL (1.064 µm)
Altitude (km)
Aerosol Optical Depth
6
5.5
5
4.5
4
3.5
3
2.5
2
1.5
1
0
0.2
0.4
0.6
0.8
1
1.2
1.4

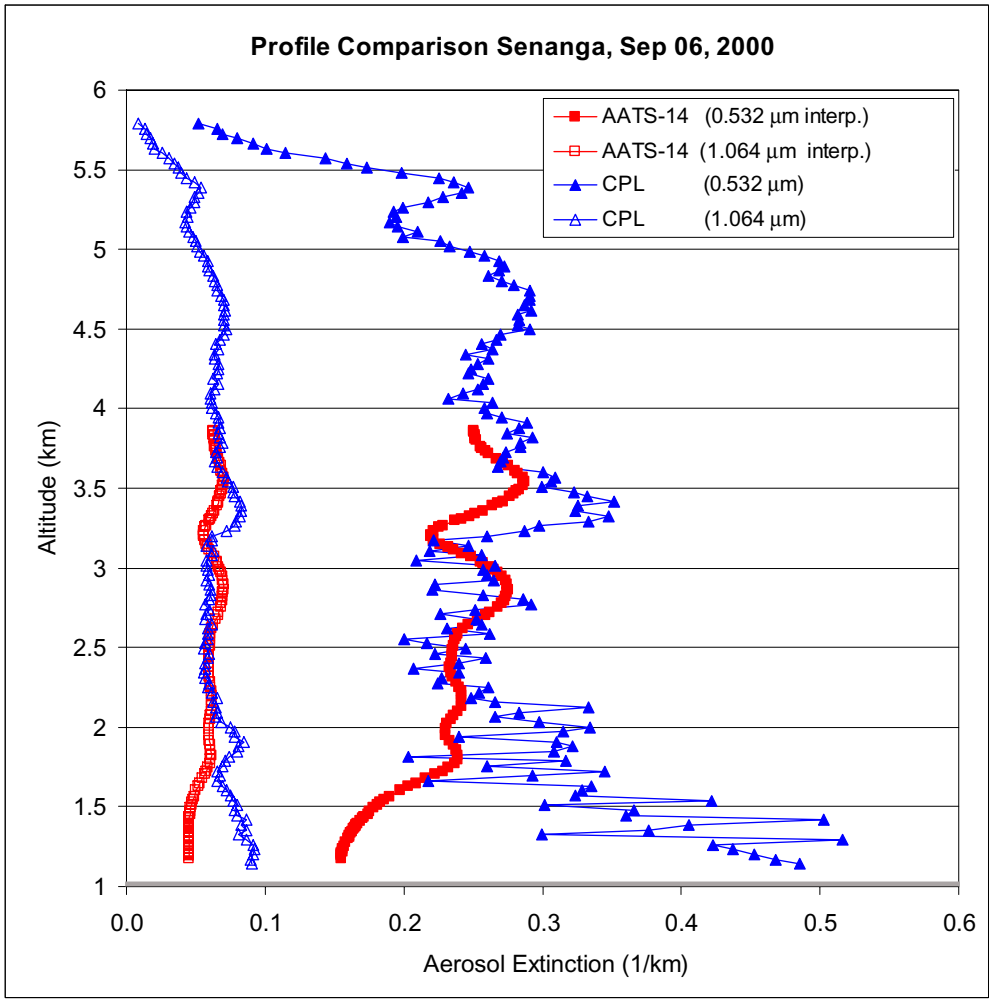
Profile Comparison Senanga, Sep 06, 2000
AATS-14 (0.532 µm interp.)
AATS-14 (1.064 µm interp.)
CPL (0.532 µm)
CPL (1.064 µm)
Altitude (km)
Aerosol Extinction (1/km)
6
5.5
5
4.5
4
3.5
3
2.5
2
1.5
1
0.0
0.1
0.2
0.3
0.4
0.5
0.6

Fig. 10

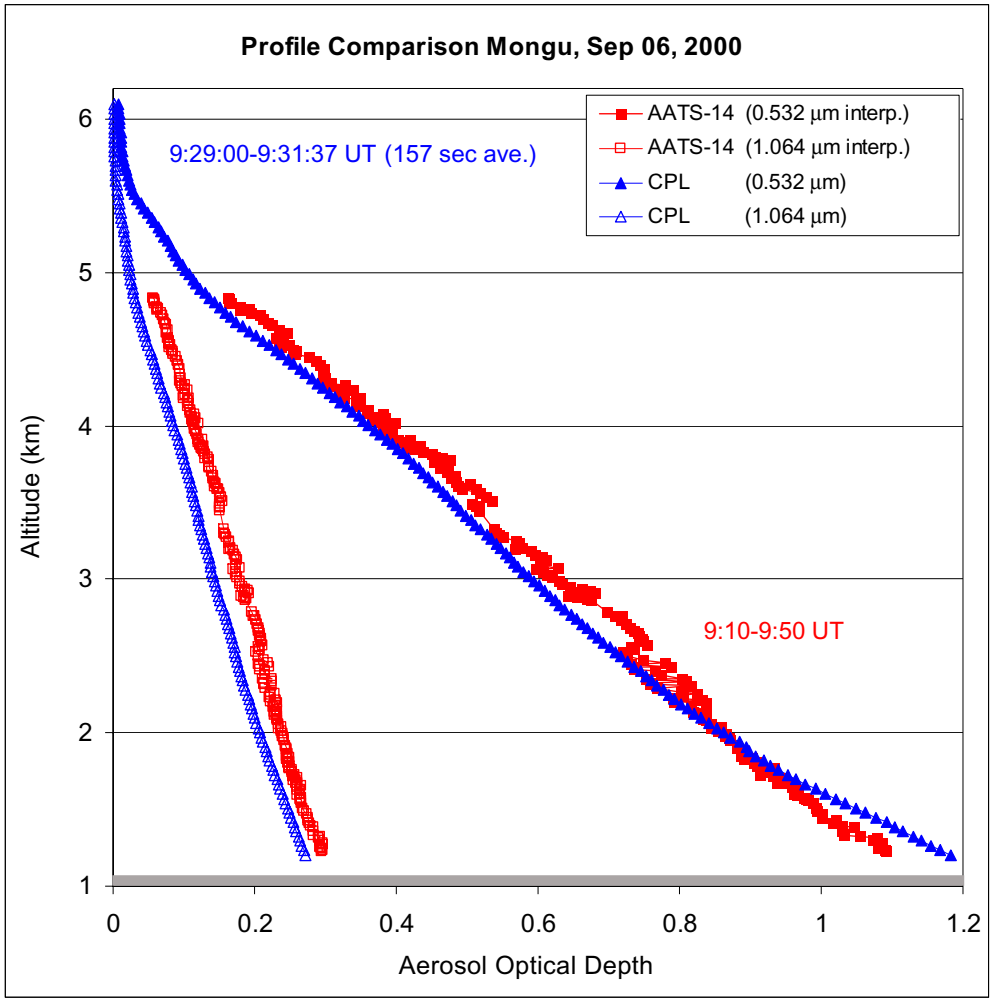
Profile Comparison Mongu, Sep 06, 2000
AATS-14 (0.532 µm interp.)
AATS-14 (1.064 µm interp.)
CPL (0.532 µm)
CPL (1.064 µm)
9:29:00-9:31:37 UT (157 sec ave.)
9:10-9:50 UT
Altitude (km)
Aerosol Optical Depth
1
2
3
4
5
6
0
0.2
0.4
0.6
0.8
1
1.2

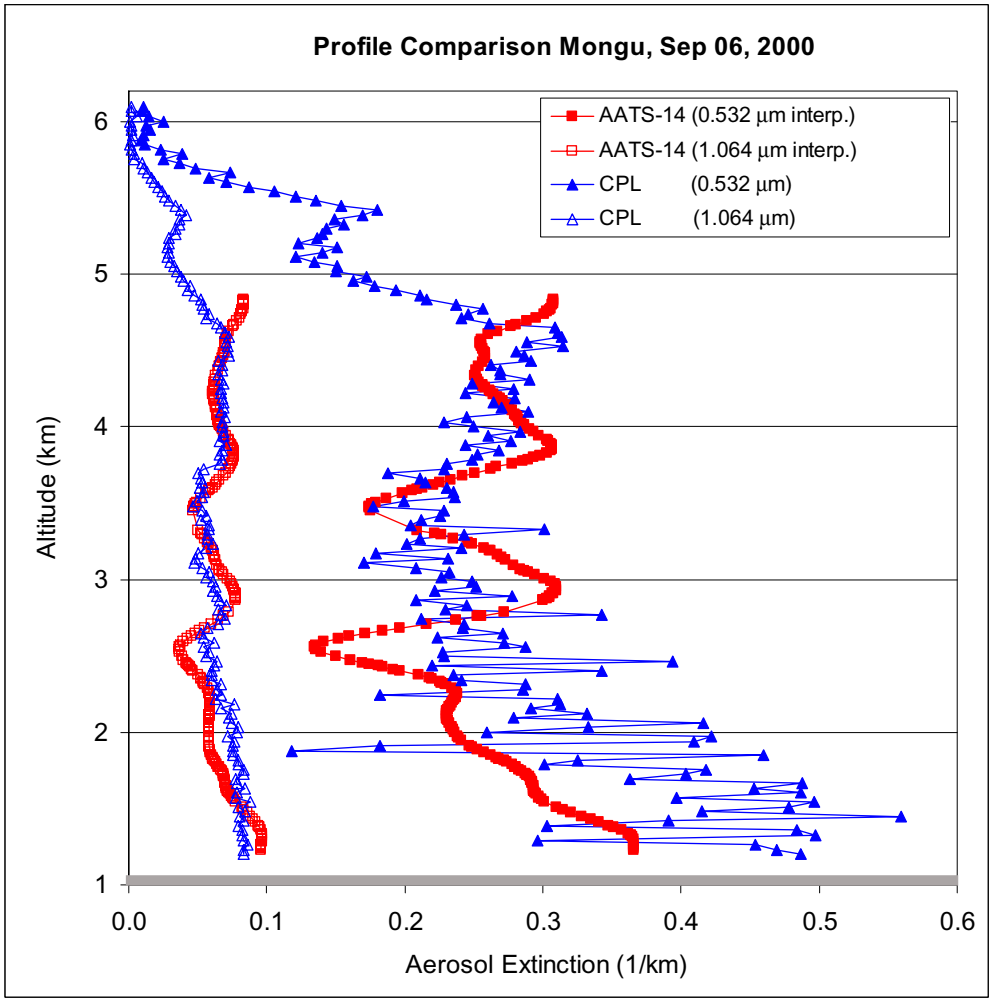
Profile Comparison Mongu, Sep 06, 2000
AATS-14 (0.532 µm interp.)
AATS-14 (1.064 µm interp.)
CPL (0.532 µm)
CPL (1.064 µm)
Altitude (km)
Aerosol Extinction (1/km)
1
2
3
4
5
6
0.0
0.1
0.2
0.3
0.4
0.5
0.6

Fig. 11

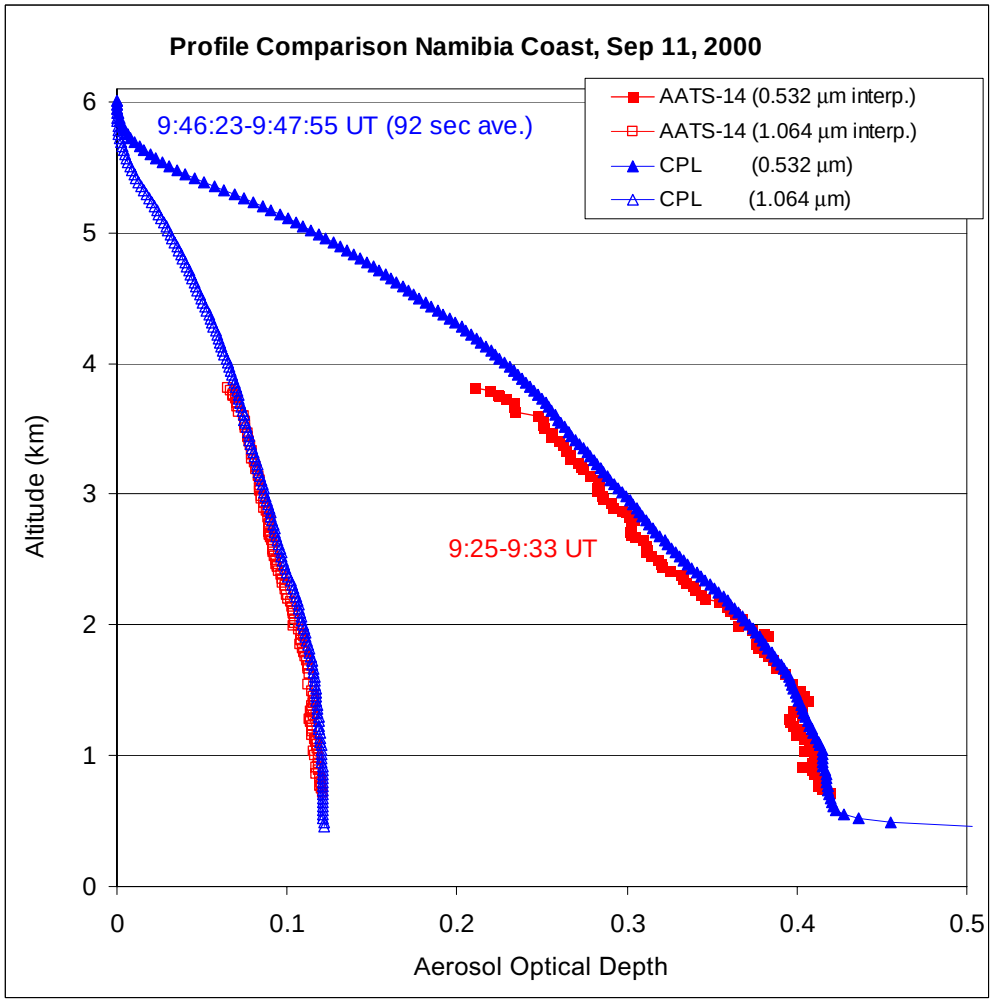
Profile Comparison Namibia Coast, Sep 11, 2000
9:46:23-9:47:55 UT (92 sec ave.)
9:25-9:33 UT
AATS-14 (0.532 µm interp.)
AATS-14 (1.064 µm interp.)
CPL (0.532 µm)
CPL (1.064 µm)
Altitude (km)
Aerosol Optical Depth
0
1
2
3
4
5
6
0
0.1
0.2
0.3
0.4
0.5

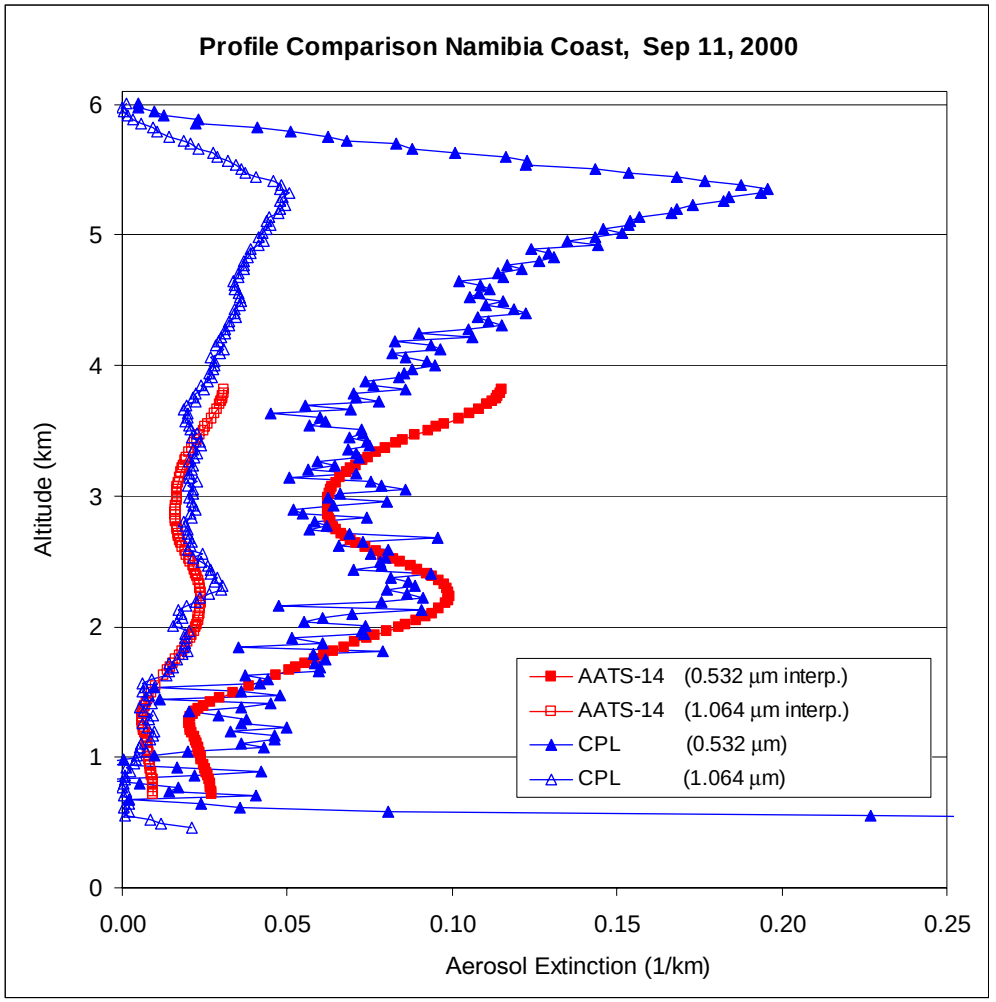
Profile Comparison Namibia Coast, Sep 11, 2000
AATS-14 (0.532 µm interp.)
AATS-14 (1.064 µm interp.)
CPL (0.532 µm)
CPL (1.064 µm)
Altitude (km)
Aerosol Extinction (1/km)
0
1
2
3
4
5
6
0.00
0.05
0.10
0.15
0.20
0.25

Fig. 12

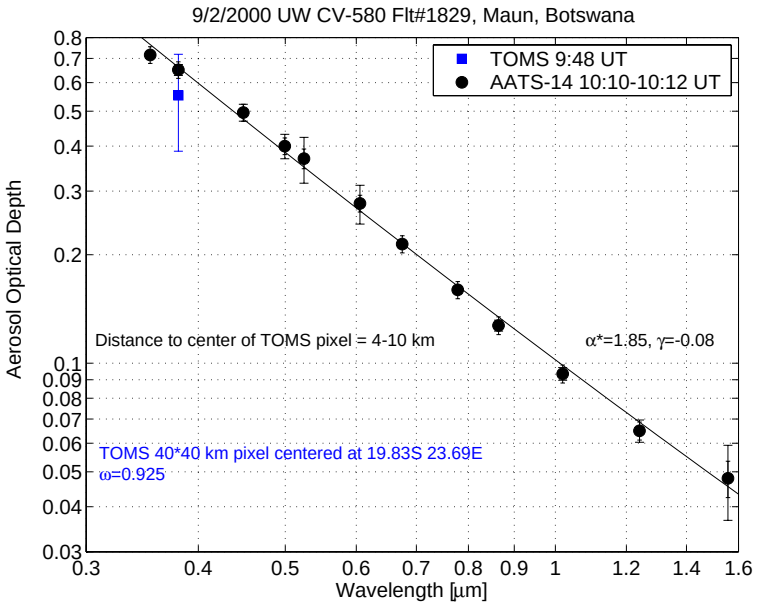
9/2/2000 UW CV-580 Flt#1829, Maun, Botswana
TOMS 9:48 UT
AATS-14 10:10-10:12 UT
Aerosol Optical Depth
Distance to center of TOMS pixel = 4-10 km
α*=1.85, γ=-0.08
TOMS 40*40 km pixel centered at 19.83S 23.69E
ω=0.925
Wavelength [μm]

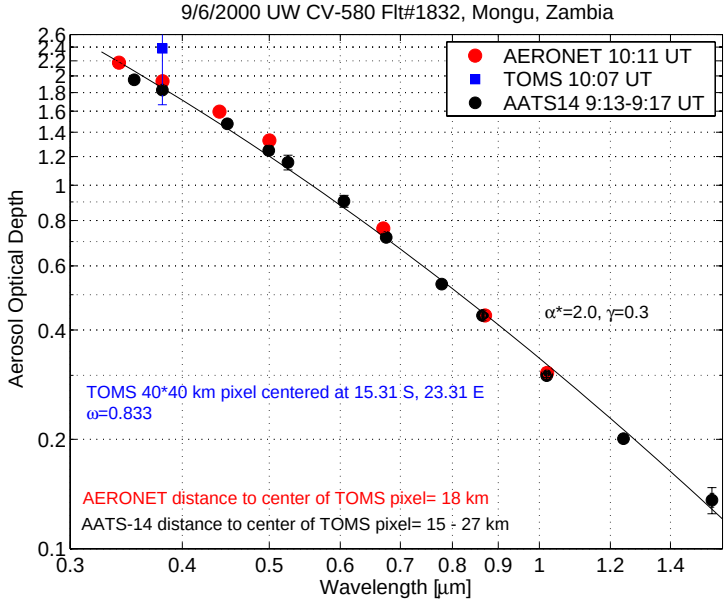
9/6/2000 UW CV-580 Flt#1832, Mongu, Zambia
AERONET 10:11 UT
TOMS 10:07 UT
AATS14 9:13-9:17 UT
Aerosol Optical Depth
α*=2.0, γ=0.3
TOMS 40*40 km pixel centered at 15.31 S, 23.31 E
ω=0.833
AERONET distance to center of TOMS pixel= 18 km
AATS-14 distance to center of TOMS pixel= 15 - 27 km
Wavelength [μm]

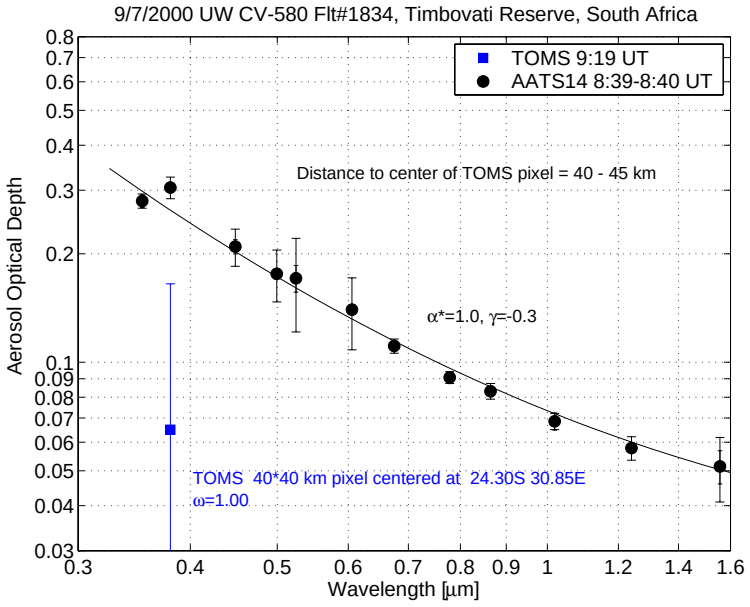
9/7/2000 UW CV-580 Flt#1834, Timbovati Reserve, South Africa
TOMS 9:19 UT
AATS14 8:39-8:40 UT
Aerosol Optical Depth
Distance to center of TOMS pixel = 40 - 45 km
α*=1.0, γ=-0.3
TOMS 40*40 km pixel centered at 24.30S 30.85E
ω=1.00
Wavelength [μm]

Fig 13

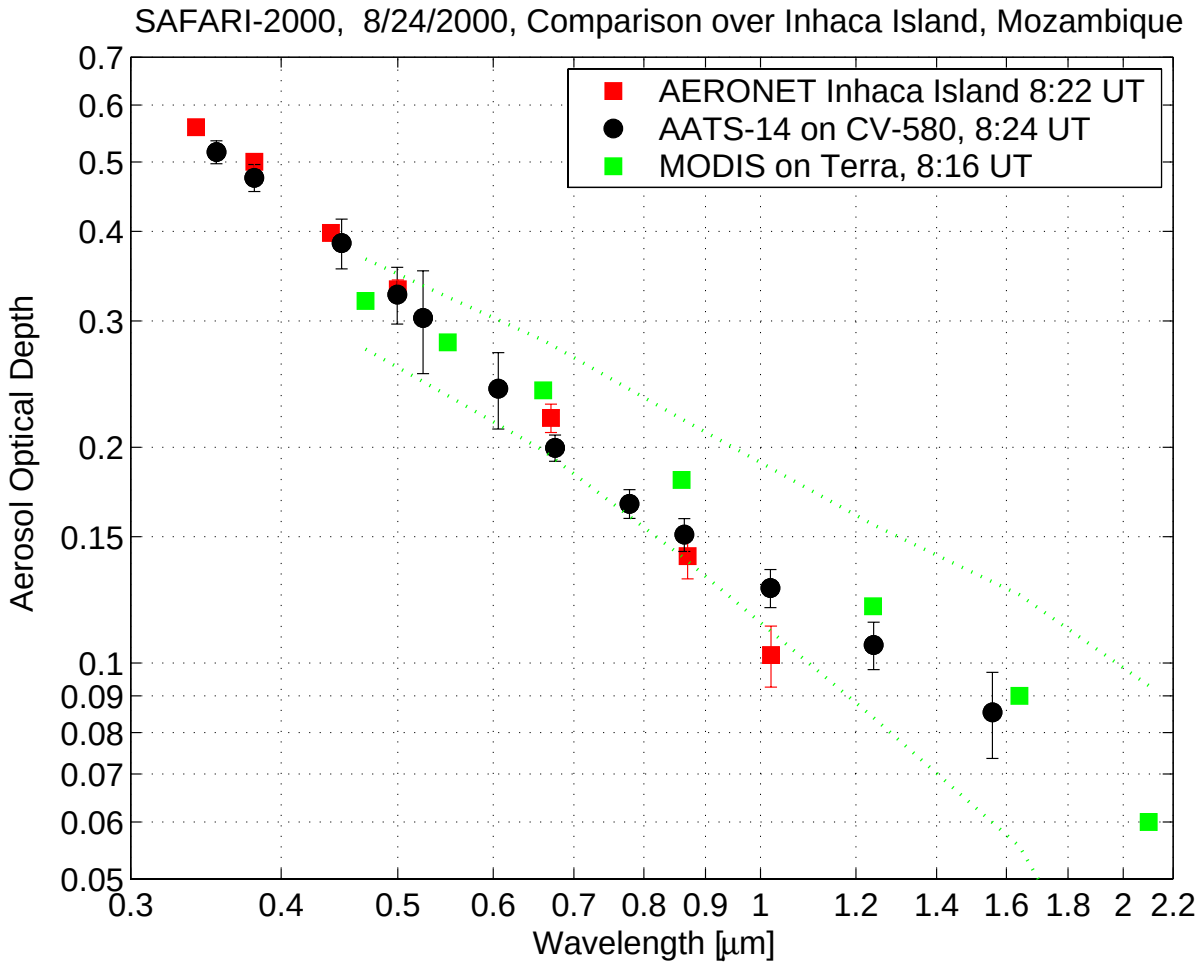
SAFARI-2000, 8/24/2000, Comparison over Inhaca Island, Mozambique
AERONET Inhaca Island 8:22 UT
AATS-14 on CV-580, 8:24 UT
MODIS on Terra, 8:16 UT
Aerosol Optical Depth
Wavelength [µm]

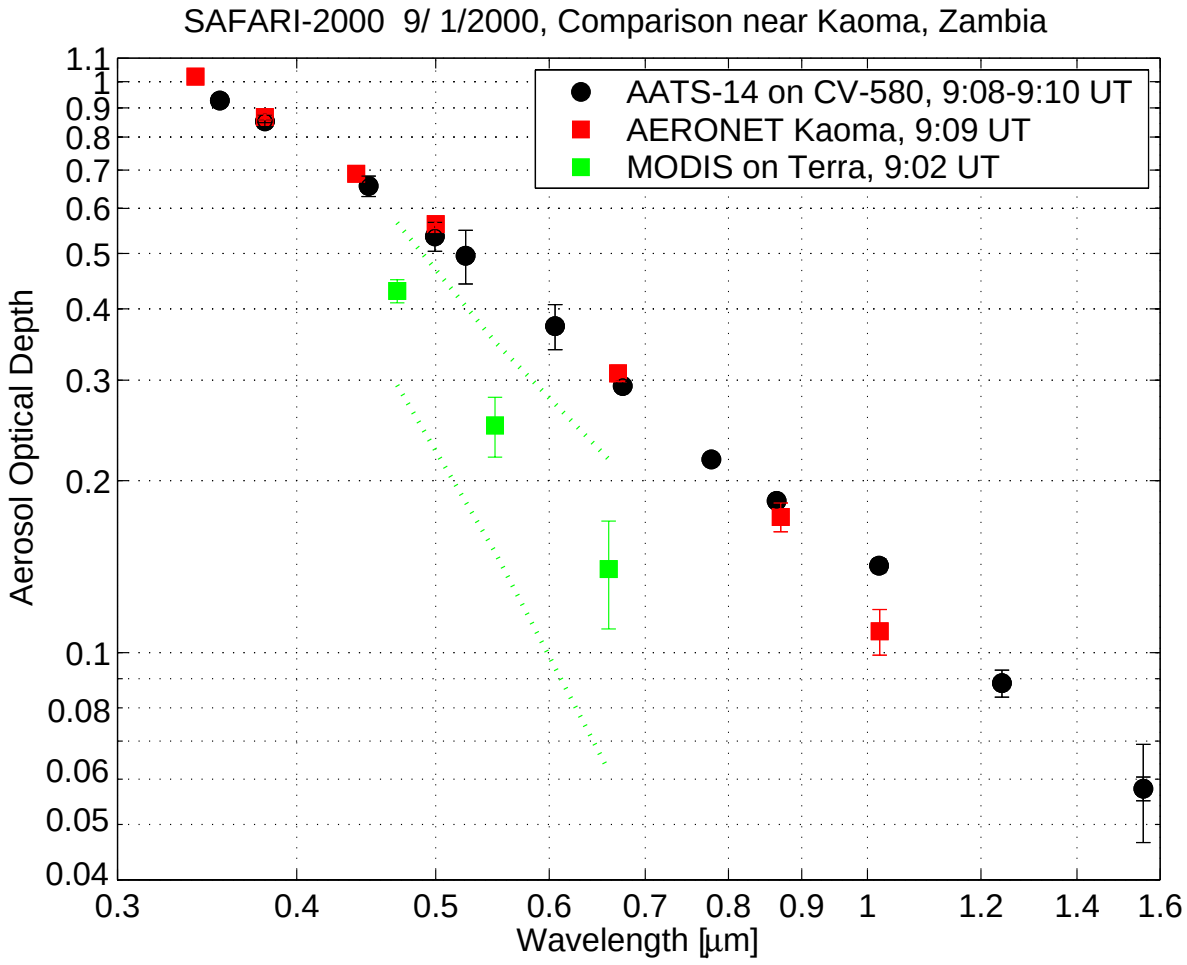
SAFARI-2000 9/ 1/2000, Comparison near Kaoma, Zambia
AATS-14 on CV-580, 9:08-9:10 UT
AERONET Kaoma, 9:09 UT
MODIS on Terra, 9:02 UT
Aerosol Optical Depth
Wavelength [µm]

Fig. 14

Fig. 15

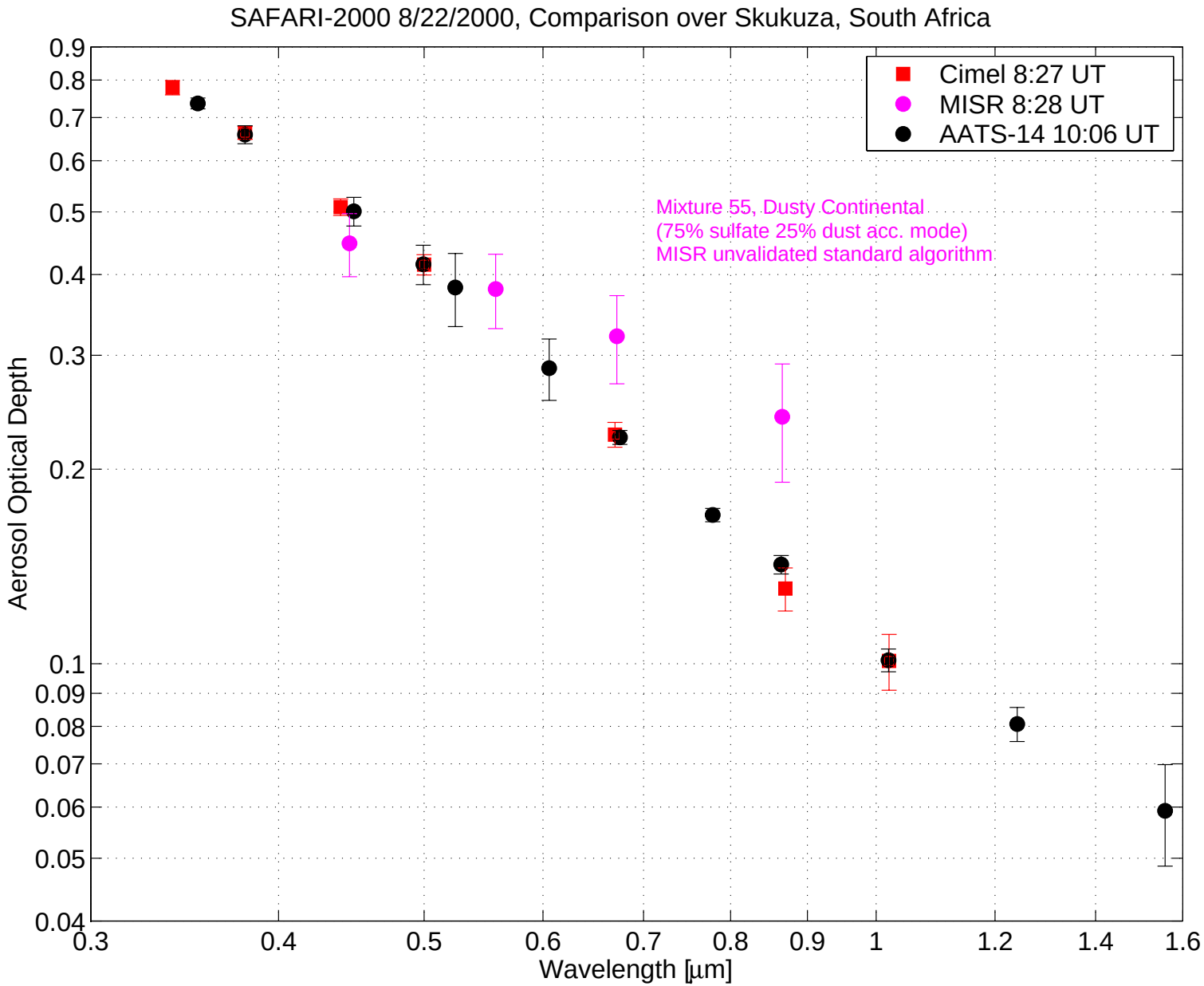
SAFARI-2000 8/22/2000, Comparison over Skukuza, South Africa
Cimel 8:27 UT
MISR 8:28 UT
AATS-14 10:06 UT
Mixture 55, Dusty Continental
(75% sulfate 25% dust acc. mode)
MISR unvalidated standard algorithm
Aerosol Optical Depth
Wavelength [μm]
0.9
0.8
0.7
0.6
0.5
0.4
0.3
0.2
0.1
0.09
0.08
0.07
0.06
0.05
0.04
0.3
0.4
0.5
0.6
0.7
0.8
0.9
1
1.2
1.4
1.6

SAFARI 2000: Orbit 3786, Blocks 107-109
September 3, 2000
MISR Level 1B2 ELLIPSOID AN(Nadir)

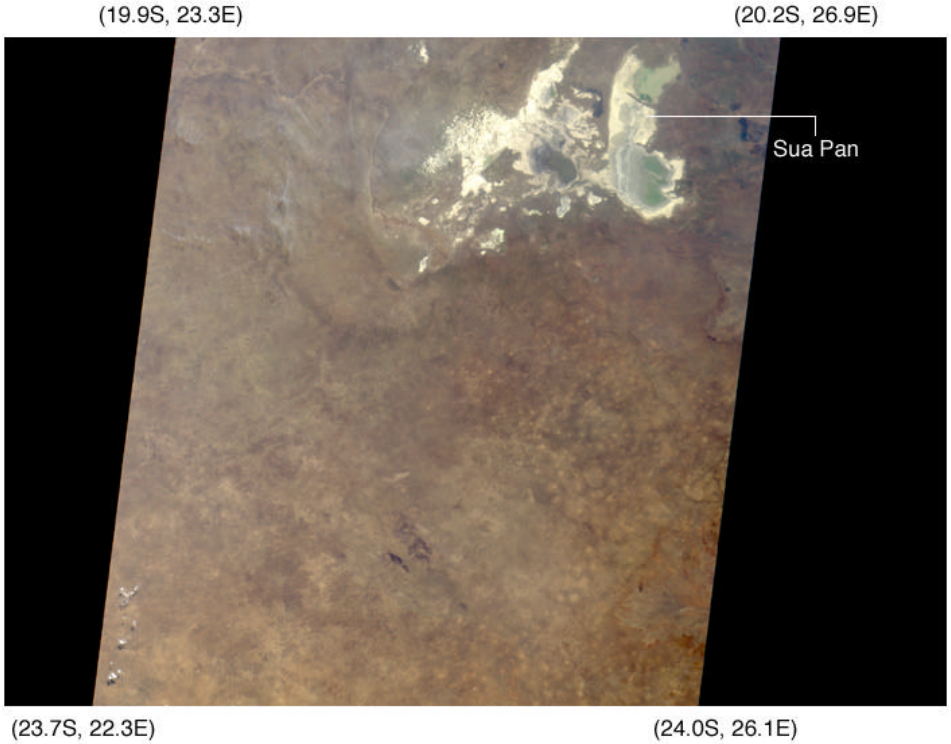

SAFARI 2000: Orbit 3786, Blocks 107-109
September 3, 2000
MISR Level 2 AEROSOL Best Fit Optical Depth

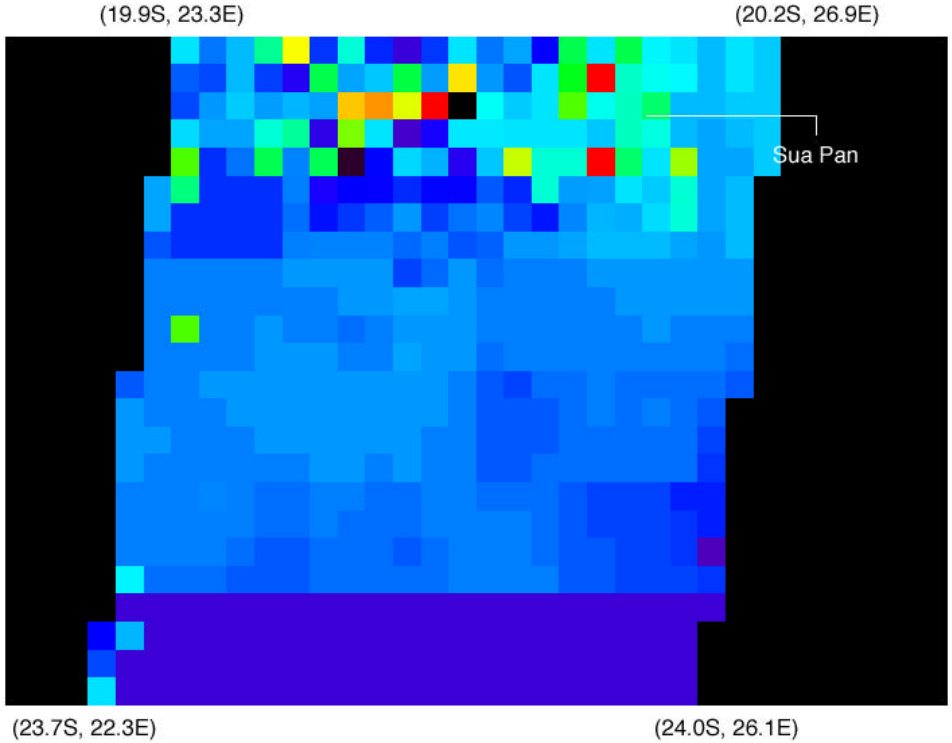

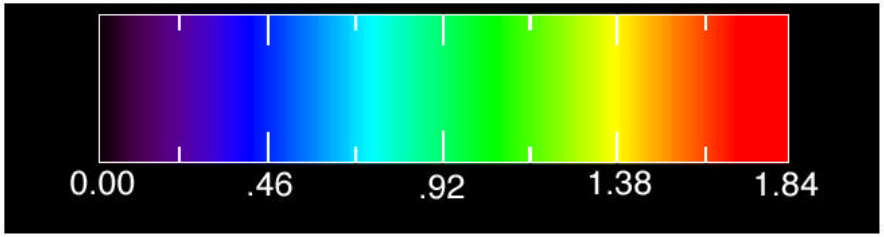

Fig. 16

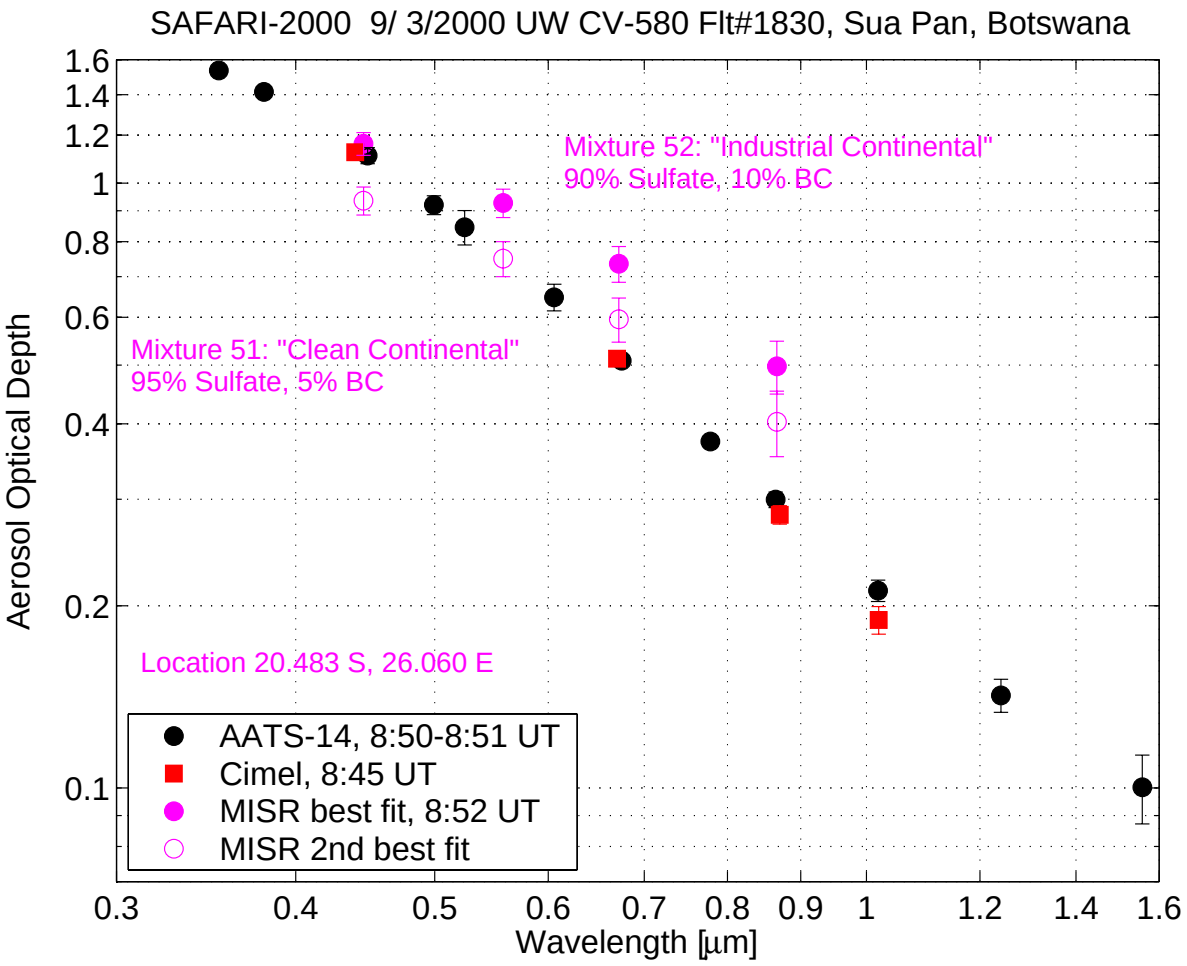
SAFARI-2000 9/ 3/2000 UW CV-580 Flt#1830, Sua Pan, Botswana
Mixture 52: "Industrial Continental"
90% Sulfate, 10% BC
Mixture 51: "Clean Continental"
95% Sulfate, 5% BC
Location 20.483 S, 26.060 E
AATS-14, 8:50-8:51 UT
Cimel, 8:45 UT
MISR best fit, 8:52 UT
MISR 2nd best fit
Aerosol Optical Depth
Wavelength [µm]

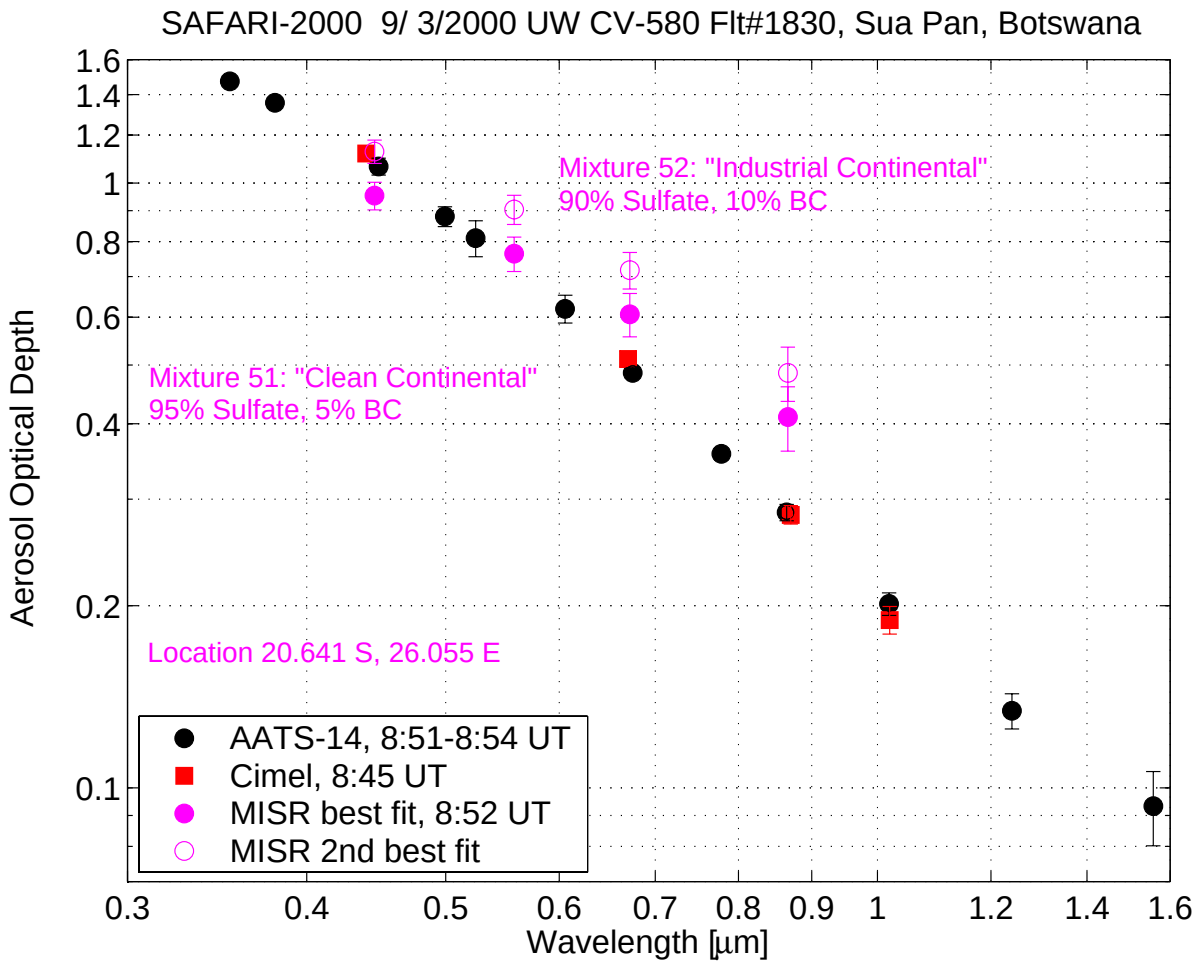
SAFARI-2000 9/ 3/2000 UW CV-580 Flt#1830, Sua Pan, Botswana
Mixture 52: "Industrial Continental"
90% Sulfate, 10% BC
Mixture 51: "Clean Continental"
95% Sulfate, 5% BC
Location 20.641 S, 26.055 E
AATS-14, 8:51-8:54 UT
Cimel, 8:45 UT
MISR best fit, 8:52 UT
MISR 2nd best fit
Aerosol Optical Depth
Wavelength [µm]

Fig 17

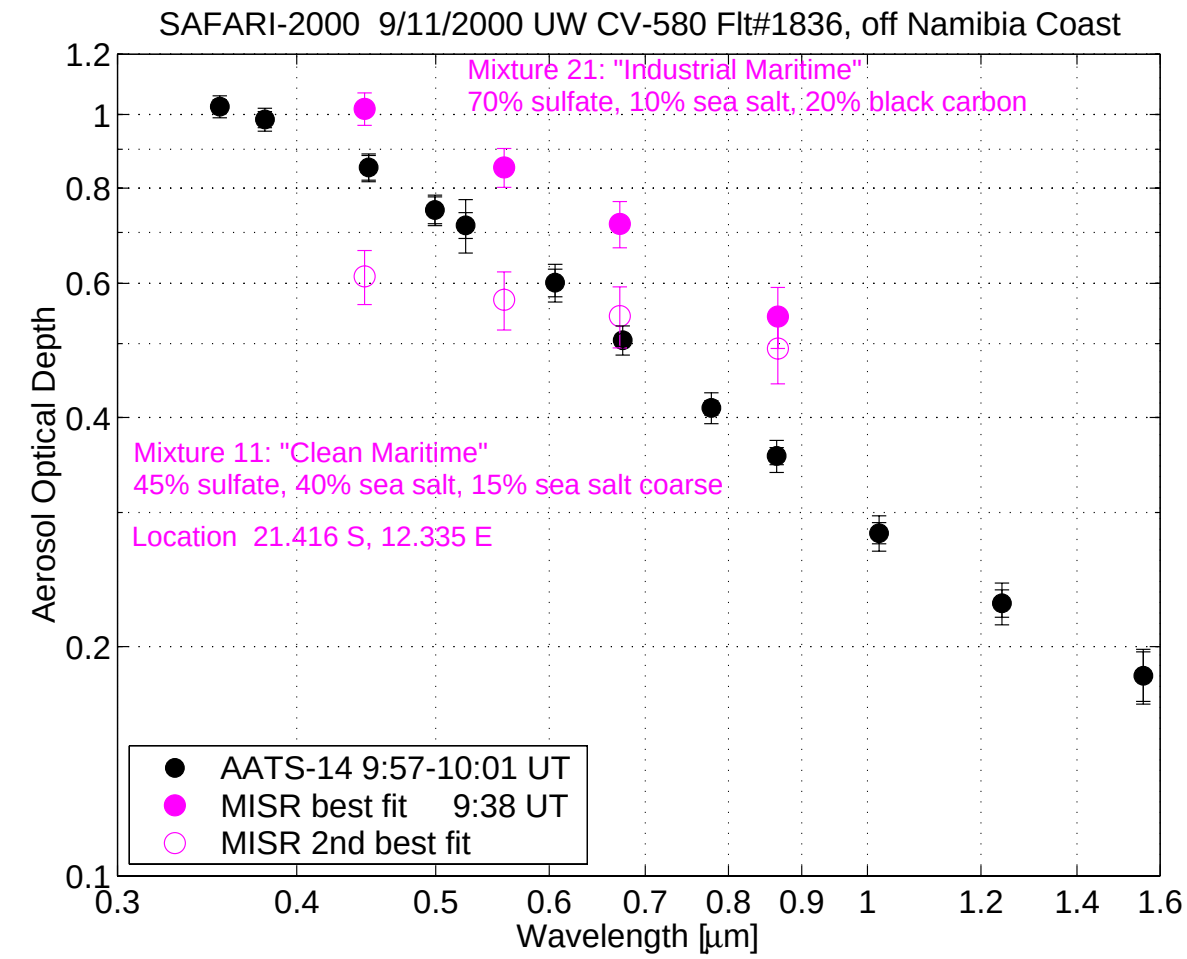
SAFARI-2000 9/11/2000 UW CV-580 Flt#1836, off Namibia Coast
Mixture 21: "Industrial Maritime"
70% sulfate, 10% sea salt, 20% black carbon
Mixture 11: "Clean Maritime"
45% sulfate, 40% sea salt, 15% sea salt coarse
Location 21.416 S, 12.335 E
AATS-14 9:57-10:01 UT
MISR best fit 9:38 UT
MISR 2nd best fit
Aerosol Optical Depth
Wavelength [µm]
1.2
1
0.8
0.6
0.4
0.2
0.1
0.3
0.4
0.5
0.6
0.7
0.8
0.9
1
1.2
1.4
1.6

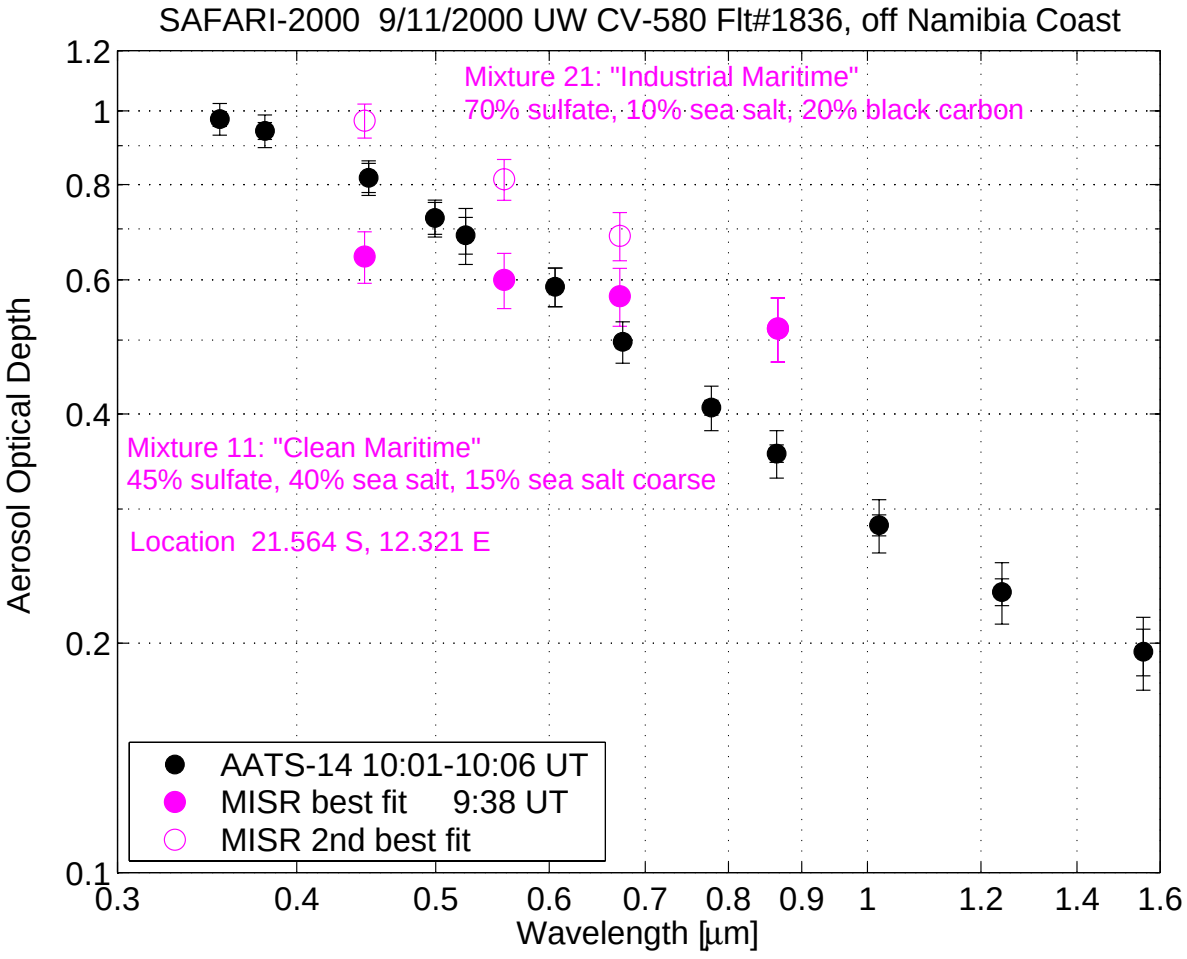
SAFARI-2000 9/11/2000 UW CV-580 Flt#1836, off Namibia Coast
Mixture 21: "Industrial Maritime"
70% sulfate, 10% sea salt, 20% black carbon
Mixture 11: "Clean Maritime"
45% sulfate, 40% sea salt, 15% sea salt coarse
Location 21.564 S, 12.321 E
AATS-14 10:01-10:06 UT
MISR best fit 9:38 UT
MISR 2nd best fit
Aerosol Optical Depth
Wavelength [µm]
1.2
1
0.8
0.6
0.4
0.2
0.1
0.3
0.4
0.5
0.6
0.7
0.8
0.9
1
1.2
1.4
1.6

Fig. 18

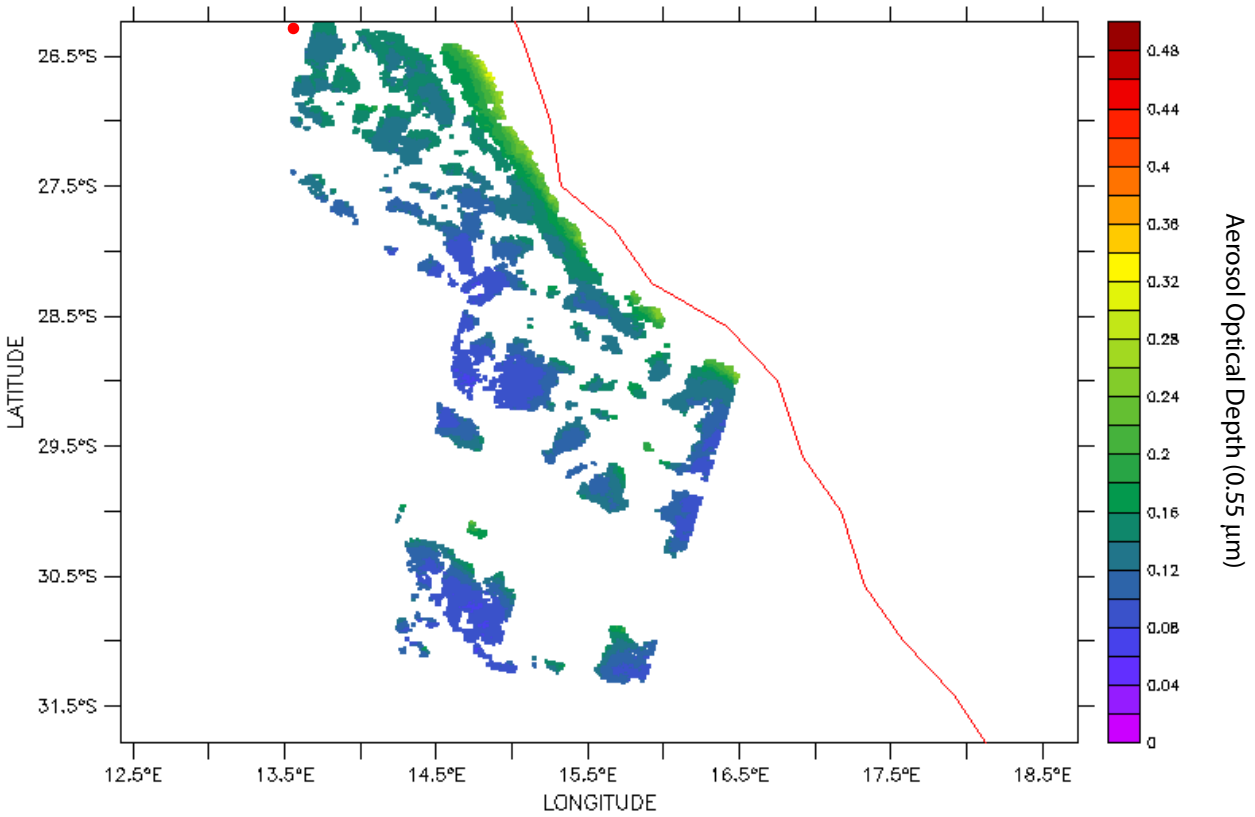
26.5°S
27.5°S
28.5°S
29.5°S
30.5°S
31.5°S
LATITUDE
12.5°E
13.5°E
14.5°E
15.5°E
16.5°E
17.5°E
18.5°E
LONGITUDE
0.48
0.44
0.4
0.36
0.32
0.28
0.24
0.2
0.16
0.12
0.08
0.04
0
Aerosol Optical Depth (0.55 µm)

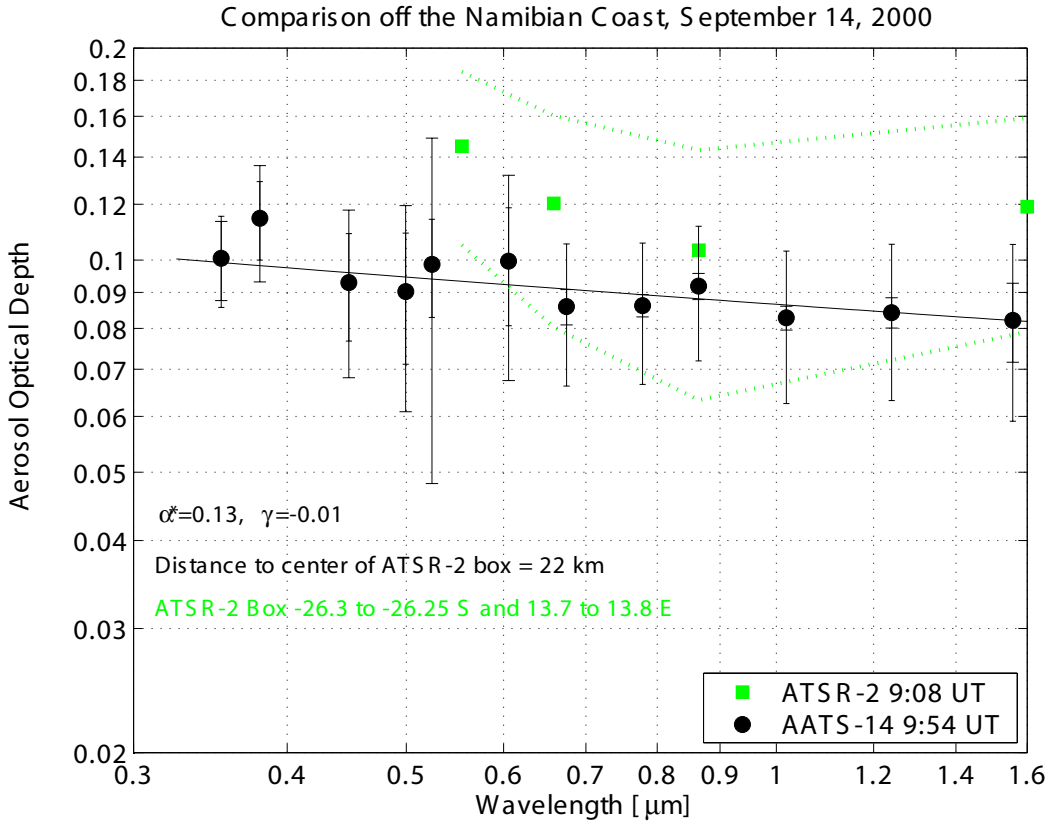
Comparison off the Namibian Coast, September 14, 2000
Aerosol Optical Depth
0.2
0.18
0.16
0.14
0.12
0.1
0.09
0.08
0.07
0.06
0.05
0.04
0.03
0.02
0.3
0.4
0.5
0.6
0.7
0.8
0.9
1
1.2
1.4
1.6
Wavelength [µm]
α*=0.13, γ=-0.01
Distance to center of ATSR-2 box = 22 km
ATSR-2 Box -26.3 to -26.25 S and 13.7 to 13.8 E
ATSR-2 9:08 UT
AATS-14 9:54 UT

Fig. 19